Undergraduate Honors Thesis:
Quantification of Brake Disc Runout Due to Assembly and Manufacturing Variations

SUBMITTED TO:

The Engineering Honors Committee

As partial requirement for graduation with distinction

in the Department of Mechanical Engineering

119 Hitchcock Hall

College of Engineering

The Ohio State University

Columbus, Ohio 43210

WRITTEN BY:

Valentina Samodelov

1437 Apt. 6 Hunter Ave.

Columbus, OH 43201

samodelov.1@osu.edu

Mechanical Engineering Department

Advisor: R. Singh

Co-Advisor: J. Dreyer

May 2010

ABSTRACT

Brake disc runout, which is defined as a variation in the distance of a brake surface to a reference plane, is a key contributor to torque variations. Runout also leads to disk thickness variation by inducing uneven wear of the disc and is affected by assembly and manufacturing inconsistencies. Dynamic frictional torques, as induced by disk thickness variation and runout, could then lead to vibrations in the seat track, steering wheel, chassis and brake pedal under high speed braking events in ground vehicles. This low frequency vibration phenomenon is often known as brake judder, and it poses customer satisfaction and warranty issues.

The purpose of this undergraduate thesis is to identify and comparatively evaluate key parameters which cause or affect runout of the brake disc. Controlled static experiments are conducted to investigate several assembly variations. Statistical analyses, including a compensation for the wide variability in the control of the bolt tightening torque, show that the bolt tightening pattern has a significant effect on runout magnitude, while indexing of the rotor with respect to the hub has an effect on the maximum and minimum runout angles. The assembly variations are also studied using a computational finite element model. The model is further utilized to investigate thermal effects of the inherent manufacturing variation of casting core shift. Qualitative analysis of the cumulative effect of core shift and heating due to friction from a braking event illustrates the significance of this manufacturing variation in its effect on both disk thickness variation and runout.

The key contribution of this thesis is a comparative evaluation of the parameters that affect runout. In particular, this work should lead to a better understanding of the assembly and manufacturing variation on brake judder and system dynamics.

ACKNOWLEDGEMENTS

1. My advisor, Dr. Rajendra Singh, for his knowledge and guidance throughout the project.

2. My co-advisor, Dr. Jason Dreyer, for his knowledge and guidance throughout the project.

3. Honda R&D.

4. The Acoustics and Dynamics Laboratory at The Ohio State University for allowing me to use their dynamometer-type setup and lab for my experiments.

5. The Ohio State University College of Engineering for providing access to the software used.

6. John Drabison for creating the brake disc model used for finite element analysis.

TABLE OF CONTENTS

LIST OF FIGURES

LIST OF TABLES

LIST OF SYMBOLS AND ABBREVIATIONS

A	Exposed heat-dissipating surface area (m^2 or in^2)
A_c	Contact area between the nut and the rotor
ANOVA	Analysis of variance
BPV	Brake Pressure Variation
BTV	Brake Torque Variation
c	Overall heat transfer coefficient ($W/m^2 \cdot °C$ or $HP/in^2 \cdot °F$)
d	Nominal diameter of the stud
DTV	Disk Thickness Variation
E	Time rate of heat dissipation (W or HP)
FEM	Finite element model
F_i	Force on the stud
GLM	General linear model
h	Overall heat transfer coefficient
LVDT	Linear variable differential transformer
$p(t)$	Brake Pressure Variation
r	Radius at measurement point
RO	Lateral Runout
t	Disc thickness
T	Tightening torue
$T(t)$	Brake Torque Variation
T_a	Air temperature in the vicinity of heat-dissipating surfaces (°C or °F)
TEI	Thermoelastic instability
T_s	Average temperature of heat-dissipating surfaces (°C or °F)
TTL	Transistor-transistor logic
v	Disk thickness variation
y	Axis perpendicular to the axis of rotation
$y(t)$	Disc thickness variation
y'	Runout axis
z	Axis of rotation
$Z(t)$	Peak-to-peak runout
Δz	Peak-to-peak runout
Z_{RI}	Runout measured from the inboard surface
Z_{RO}	Runout measured from the outboard surface
α	Runout angle
φ	Coning angle

1. INTRODUCTION

1.1 MOTIVATION

Brake judder is defined as a vibration during high speed braking events, proportional to the vehicle speed and perceived by the driver through the seat track, steering wheel, chassis and brake pedal [1-6]. It occurs during braking events at speeds above approximately 60 mph and has low frequency content, on the order of 10-20 Hz [1, 2]. Brake judder is caused by, and usually measured through, the brake torque variations (BTV), T(t), and brake pressure variations (BPV), p(t), in tests using a brake dynamometer. In disc-caliper systems, some of the contributing causes of T(t) and p(t) are misalignment of the rotor with respect to the caliper, uneven heating of the disc, changes in frictional contact, elastic deformation, uneven wear, and disc thickness variation (DTV) [3]. Customer satisfaction and warranty issues require that we seek a better understanding of the underlying causes including the run out.

This thesis focuses on quantifying runout of the rotor disc due to assembly and manufacturing variations of the rotor. In the case of a brake rotor, there are two surfaces, an inboard and outboard surface, as shown in Figure 1. While runout can be measured in a variety of ways, one method is using a dial indicator mounted on the frame to measure the peak-to-peak variation of the inboard surface of the rotor while turning the rotor one full revolution. Runout, or z(t), leads to increased DTV, y(t), by allowing a regular contact between the pad and disc surface outside of braking events and uneven contact pressure during braking events [4].

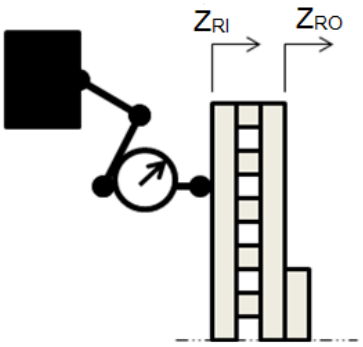

Figure 1: Measurement of disc runout. Here Z_{RI} is the runout of the inboard rotor surface, and Z_{RO} is the runout of the outboard rotor surface (hat side).

Further, the lateral runout (RO) is defined as a variation in the distance of a surface from a reference plane perpendicular to the axis of rotation. It can also be quantified by the angle, α, between the runout axis, y', and the axis perpendicular to the axis of rotation, y. Figure 2 illustrates these two methods of quantifying lateral runout.

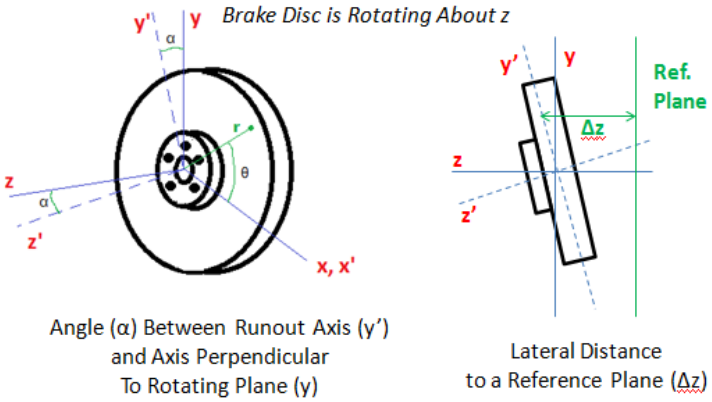

Figure 2: Runout quantification by angle α (left) and distance to a reference plane (right)

The DTV or *v*, in turn, is defined as a variation in thickness of the friction surface of a disc [4]. While DTV has been accepted as a leading contributor to brake judder, the effect of runout on brake judder has not been explored as extensively. Using Figure 2, the relationship between runout (Z_{RI}) and DTV (*v*) is described by the following equation [7], where *t* is the thickness of the disc and *r* is the radius at the measurement point.

$$\frac{v}{v} = \frac{1}{\cos\alpha} - 1 = \frac{1}{\sqrt{1-(Z_{RI}/2r)^2}} - 1 \qquad (1)$$

1.2 RESEARCH SCOPE AND OBJECTIVES

Although runout is yet to be regarded in scientific literature [1, 4, 5] to be as significant an input to brake judder as DTV, runout leads to uneven wear of the disc surfaces and ultimately a variation in thickness. Runout can be caused by either manufacturing or assembly variations or defects [2]. Figure 3 shows the difference between manufacturing and assembly runout. Initial runout of an installed disc, incorporating manufacturing and assembly variations, is usually between 40 and 100 µm [4, 6, 8].

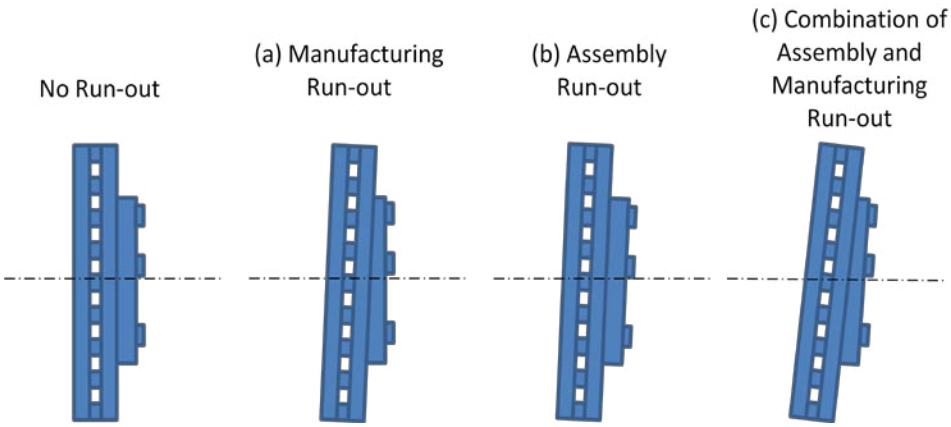

Figure 2: Causes of runout. (a) due to manufacturing, (b) due to assembly, or (c) due to a combination of both assembly and manufacturing.

Unlike DTV, which is a property of the rotor disc alone, runout depends on the assembly or the boundary conditions imposed on the disc-caliper system. Even for the same rotor and hub combination, a different level of system runout is likely to be measured for each assembly, where changes to the bolt torque and orientation of the rotor with respect to the hub will affect runout. This project will quantify key conditions or parameters that affect runout on the dynamic friction lab experiment in the Acoustics and Dynamics Laboratory at The Ohio State University, which serves as a judder dynamometer. Quantification of the range of runout, due to different parameters, could explain variations in

measurements and should lead to an improved understanding of brake systems and models of the brake judder phenomenon.

The main objective of this thesis is to quantify runout in order to adjust future models based on this experiment. This will be accomplished through experimental tests as well as finite element analysis. The main intent of the experimental portion is to quantify the effect of various parameters on runout; it is conducted via a series of static experimental runs on a disc brake rotor. The experimental results will be compared to those of the finite element model (FEM) in order to better understand the underlying causes and to partially validate the FEM. The effect of the manufacturing defect of core shift in conjunction with heating due to braking events on runout will be investigated using FEM. This research project should lead to an improved measurement or characterization procedure which could be used for future projects.

2. MANUFACTURING RUNOUT

2.1 PROBLEM FORMULATION

2.1.1. Quantification of Manufacturing Runout

Runout is inherent to current brake disc manufacturing processes, despite quality controls in place to minimize this variation. Since more emphasis is placed on the effect of DTV on brake judder, an installed brake disc typically has runout on the order of 40-100 µm, while DTV is more tightly controlled, say up to 6-10 µm [6]. Typically, manufacturing runout is quantified by mapping the rotor prior to installation. This is completed by measuring the distance to the back surface of the rotor with a coordinate-measuring machine (CMM), or using another measuring system, at various radii and in certain degree intervals [2]. Practically, this type of measurement is not completed on most rotors installed in automobiles. Instead the brake disc is mounted horizontally onto a test stand and spun to

detect imbalances. These are countered by machining a groove, known as the balancing mark, into the edge of the brake disc between braking surfaces. A picture of a balancing mark can be seen in Figure 4.

Figure 3: Balancing mark - used to counteract manufacturing variations in the brake disc

2.1.2. Variation of Core Shift in Manufacturing

Core shift is a manufacturing variation characterized by a tilting or displacement of the core during casting of the brake disc [9]. The core is a piece of the mold that is removed after casting and creates the open space of the veins between the two braking surfaces of conventional brake discs. It is caused by an assembly issue of the mold, leading to misalignment of the core in most brake discs. Core shift leads to a variation in the thickness of the braking surfaces. A conceptual diagram showing the effect of core shift on the braking surface thickness can be seen in Figure 5.

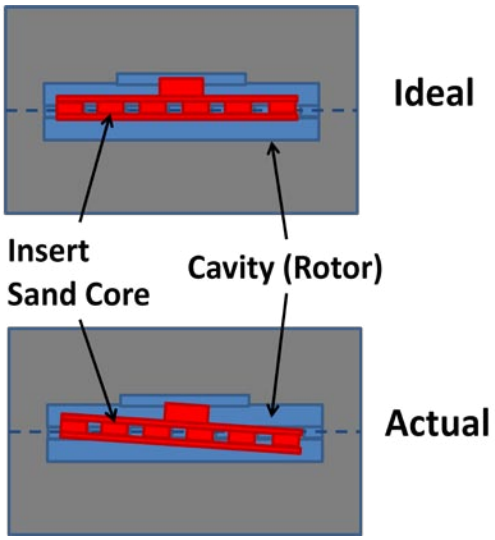

Figure 4: Example of how core shift can affect brake surface thickness

Since core shift affects the interior of the brake disc, rather than the braking surfaces of the rotor, using a mapping procedure on the outside surfaces would not detect this defect. However, the uneven distribution of material is detected in the horizontal spin quality test and "counteracted" by the balancing mark.

2.1.3. Heating Due to Friction

During braking events, heat due to friction between the caliper pads and braking surfaces of the disc is transferred into the rotor. Energy dissipated in disc brakes in time *dt* follows the relationship [10]:

$$dE = hA(T_s - T_a)dt \qquad (2)$$

Where *E* is the energy dissipation, *h* is the overall heat transfer coefficient, *A* is the exposed heat-dissipating surface area, T_s is the average temperature of heat-dissipating surfaces and T_a is the air temperature in the vicinity of the surfaces. In extreme cases, braking events can cause rubbing speeds up to 22 m/s with a pressure of 10 MPa, which causes temperatures at the disc surface to rise up to 800°C [8]. In high speed repeated braking events, such as those where judder is apparent, the heat transferred to the brake disc is in the 8 - 16 MW range [11]. Due to geometry variations in the disc, this heating is rarely uniformly distributed and uneven heating leads disc warping and coning, localized

thermal expansion, phase transformations and pad material deposits from the brake pads to the rotor [3]. All of these could be judder contributing factors.

Intense heat generation could lead to thermo-elastic instability (TEI) under rare conditions [3, 11, 8]. Heat generation also creates hot spots, or areas of the brake disc surface where heat is concentrated at temperatures around 200 – 250 °C above surrounding surfaces [3]. Hot spots can lead to phase changes in the rotor, causing these already raised parts of the disc to become more pronounced [3, 11, 8]. Consequently more uneven friction regimes may emerge as a result of enhanced caliper contacts.

Another prominent result of the thermal effects of friction is coning of the brake disc. This is an affect due to the geometry of the disc and causes the braking surface of the disc to rotate away from the bearing [12]. Figure 6 shows how the coning angle is defined. Hot spots, coning and other thermal deformations could enhance add the DTV in the rotor, which causes BTV as well as “hot judder” [8].

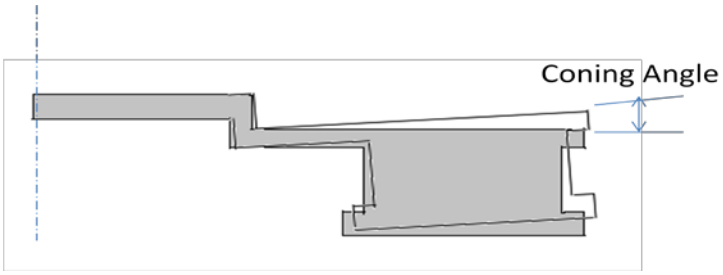

Figure 5: Diagram illustrating the definition of coning angle

2.1.4. Fundamental Questions

While the core shift itself does not lead directly to manufacturing runout, friction-induced heating of the rotor in conjunction with core shift should induce uneven wear that causes runout and DTV. The finite element model (FEM) analyses conducted in this research project is intended to qualitatively analyze the effect that the manufacturing variation of core shift has on runout, coupled with heating due to braking friction. Simulating wear is clearly outside the scope of this project, so

model runout is numerically “measured” as a result of static heating of the disc braking surfaces at different conditions of core shift. The fundamental questions that have been posed include:

- Does core shift have an impact on runout when coupled with brake-friction heat?
- At what level of heating does core shift become a significant contributor to runout?
- What conditions of core shift have the greatest effect on runout?
- Is the runout caused by uneven heating as a result of core shift significant when compared to the assembly runout?

2.1.5. Finite Element Model Assumptions

In order to create a model for assessing the effect of core shift, coupled with friction heating, several assumptions are made. The effects of these assumptions are as follows:

- An ideal disc with no runout or DTV present prior to application of the temperature gradient is modeled.
- Heating due to friction is assumed to be distributed evenly on both braking surfaces.
- A uniform temperature distribution is used– vein cooling due to disc rotation and any gradient due to the presence of calipers are ignored.
- The center of friction is taken to be at the center of the braking surface.
- Convection around the rotor is neglected.

2.2 STATIC AND THERMAL CALCULATIONS

2.2.1. Modeling Core Shift

A simplified model of the core shift is created in order to do a qualitative analysis of the effects of core shift coupled with heating. A SolidWorks model of a representative brake disc of a 2000 kg vehicle is modeled and used for baseline analysis in this experiment. Instead of tilting the core, material is added or removed uniformly from each surface with the total thickness of the rotor remaining

unchanged. While core shift usually manifests as a tilting of the core rather than a uniform lateral displacement, this analysis method qualitatively shows the effects of core shift coupled with friction induced heating during braking events.

A baseline with no core shift is used a reference for the normalized data, while other models varied between inboard and outboard core shift up to 1.5 mm. Figure 7 is a diagram showing the coordinate system and core shift naming conventions. A core shift towards the outboard surface is taken as positive, while inboard core shift is negative. The total distance between the braking surfaces remains a constant 27.96 mm since this is the initial thickness of the SolidWorks model. Inboard core shift is a displacement of the core towards the inboard braking surface, making t_i smaller than t_o and denoted by negative numbers. Outboard core shift is a displacement towards the outboard rotor surface, with t_o becoming the thinner thickness and denoted by positive numbers.

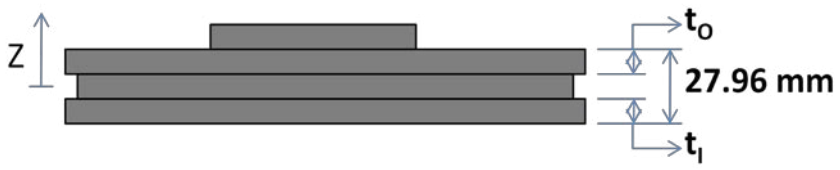

Figure 6: Coordinate system and naming conventions used for modeling core shift

2.2.2. Thermal Analysis

SolidWorks Simulation is an FEM tool integrated into SolidWorks and has the capabilities required to complete a comparative analysis of the effect of core shift, coupled with friction heating, on runout. The SolidWorks model is constrained with boundary conditions based on a dynamometer test setup. Figure 8 shows the model with the mesh and loading scheme. The back of the hub is constrained with a zero translation flat surface fixture, representing a stiff bearing. The five bolt holes are constrained with zero translation cylindrical surface fixtures, representing stiff bolts with even tightening. Both the inboard and outboard braking surfaces have constant and evenly applied thermal loads. The mesh size is 5 mm with a 0.25 mm tolerance.

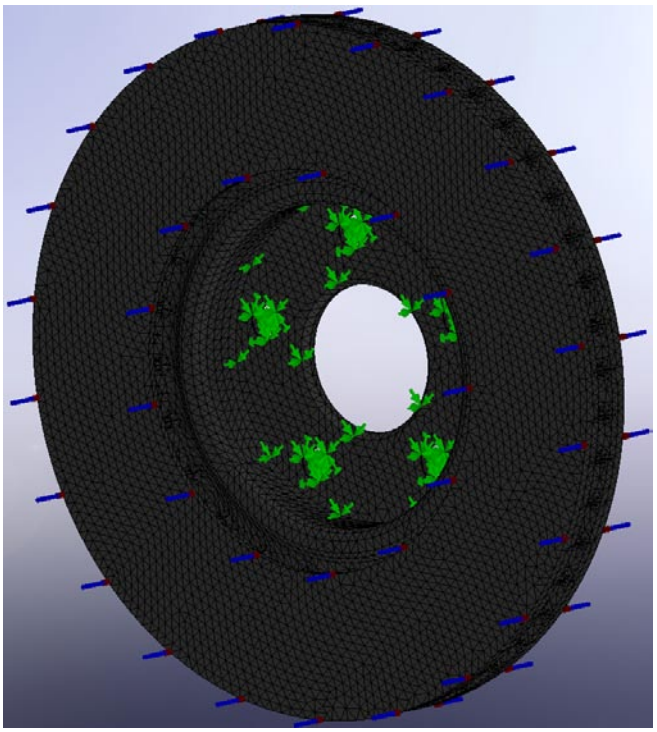

Figure 7: FEM with 5 mm mesh, constant temperature load across both braking surfaces, and zero translation fixtures at the bolt holes and back of the hat surface

In order to quantify the correlation between temperature and core shift, two different analyses are completed. The first analysis covers different values of core shift at a baseline temperature. During experimental testing of a brake disc D. Bryant et al. found audible judder at 150° C, with significant BPV beginning at 300°C, so 150°C is selected as the baseline for our core shift finite element analysis [11]. The second analysis varies temperature at a core shift of 1.0 mm towards both the inboard and outboard surfaces. The maximum temperature numerically tested is 200 °C.

Experimental measurements of the displacement in the z direction are taken on both the inboard and outboard braking surfaces, along the center of friction, using the probe. The runout measured on both sides of the rotor is then averaged to create data points for each braking surface.

2.3 RESULTS AND DISCUSSION

The geometry of the rotor causes an uneven displacement of the inbound to outbound rotor surfaces. A screen shot of the displacement in the z direction, exaggerated for display purpose by SolidWorks Simulation, can be seen in Figure 9. The first image shows the cross section through the vein of the rotor prior to running the simulation; notice the profile angles connecting the hat to the braking surfaces. The second image is shown as a reference to show the colors corresponding to z displacement in the rotor. Red corresponds to the least displacement, occurring at the hat which was held by boundary conditions. The greatest displacement occurred in the edges of the braking surface and is denoted by blue. The displacement profile shows coning. This is qualitatively consistent with other computational and experimental thermal studies on brake discs [8, 11].

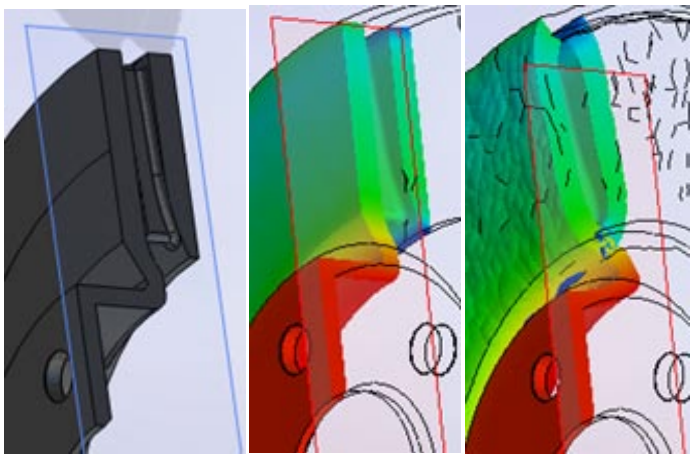

Figure 8: Screen shots of rotor displacement due to heating effects; from left to right: rotor profile prior to analysis, profile showing colors corresponding to z displacement and deformed result, with red denoting no displacement and blue correlating to the greatest displacement

In order to quantitatively evaluate the effect of core shift on coning due to thermal effects, plots across both the inboard and outboard braking surfaces are created on a radial line over one half of the rotor. These plots, depicted in Figure 10, show a comparison of coning angle at no core shift, 1 mm core shift and -1 mm core shift, under a uniform thermal load of 150 °C across both braking surfaces. Inboard core

shift creates a noticeably greater coning angle than outboard core shift, as compared to the no core shift model.

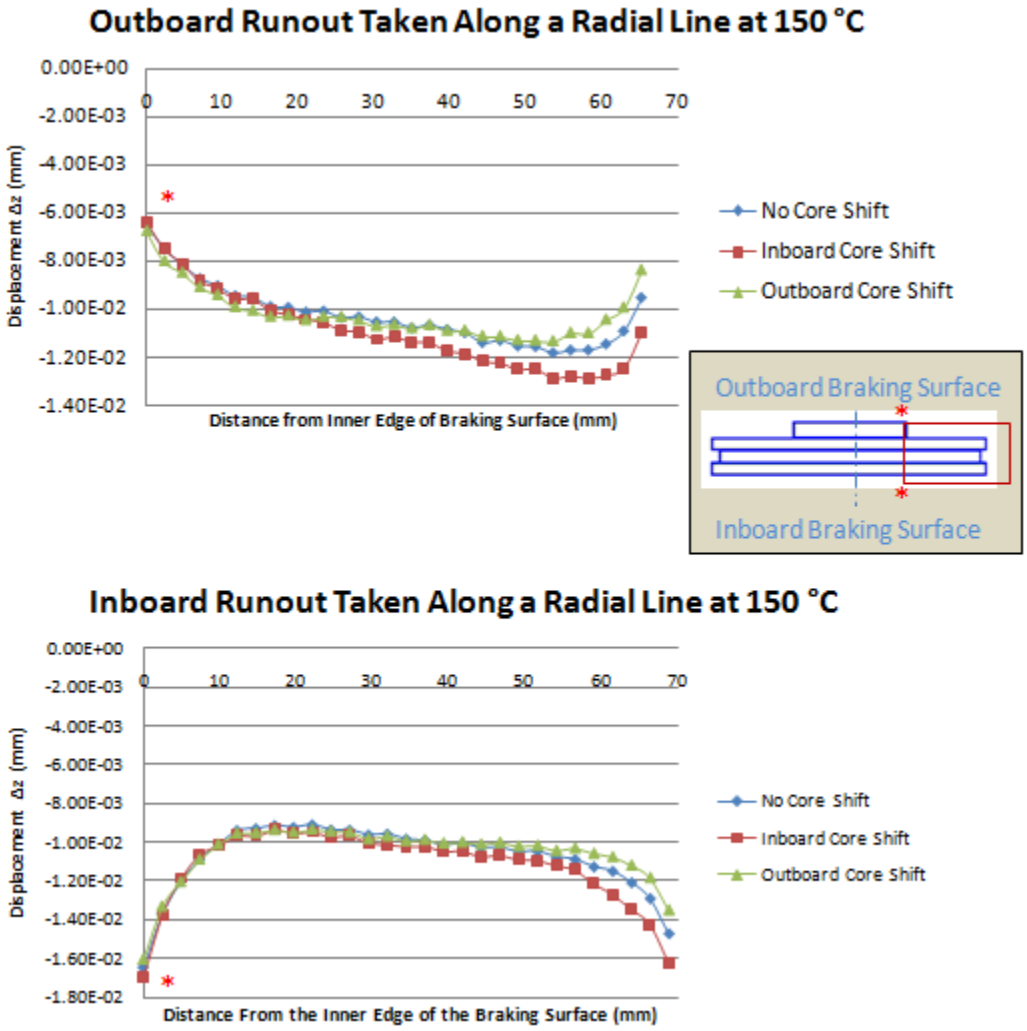

Figure 9: Temperature profiles along a radial line of the brake surface at a thermal load of 150 °C at three different levels of core shift

Table 1 shows a comparison of the approximate coning angle for inboard and outboard core shift, compared to the no core shift model. Core shift of 1.0 mm towards the outboard surface of the rotor shows about 50% of the angular displacement of a perfect rotor, while inboard core shift shows a much greater coning angle.

Table 1: Comparison of runout in models showing core shift towards in the inboard and outboard surfaces normalized to a zero core shift model

Core Shift	Measurement Surface	Normalized Coning – φ (°)
Outboard 1.0 mm	Outboard	56.90%
	Inboard	54.10%
Inboard -1.0 mm	Outboard	146.60%
	Inboard	120.50%

This result would indicated that brake disc manufacturers focusing on minimizing thermal coning in brake discs should design their rotors with a slight outboard core shift. However, this may not be practical or desirable for decreasing other judder contributing factors, so a focus on minimizing inboard core shift may simply be more important to reduce runout.

Two analyses are completed to assess the relationship thermal load and core shift have with runout. The first varies temperature from 40 – 200 °C, while keeping core shift constant at -1.0 mm and 1.0 mm. Figure 11 shows the resulting z displacement on both the inboard and outboard surfaces. The data has been normalized against the perfect rotor model, with no core shift.

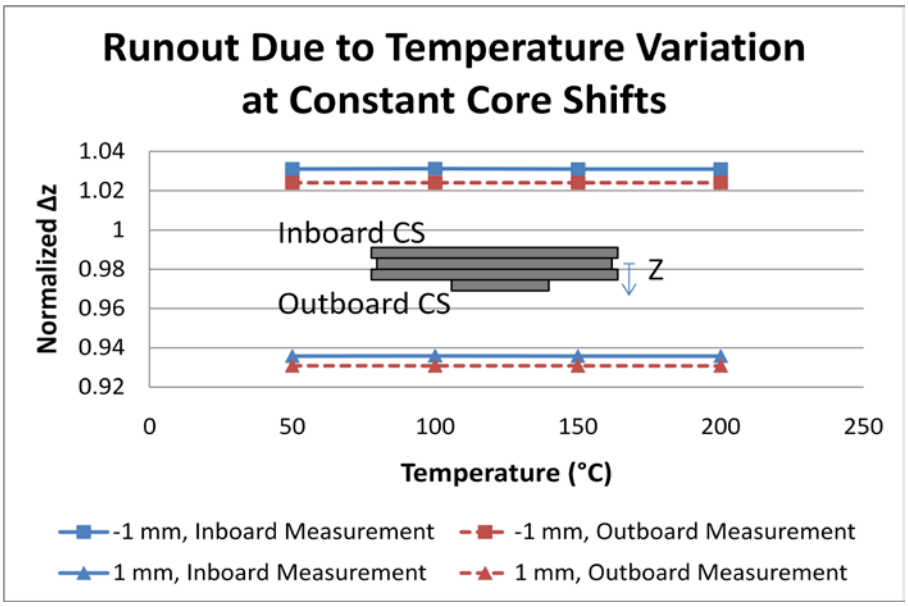

Figure 10: Result of varying temperature at a constant core shift, normalized against data from a perfect rotor with no core shift

This model indicates that varying temperature has little to no effect on the magnitude of thermally induced runout due to core shift. It should be noted that, although both the inboard and outboard core shift models show increasing runout with greater temperature loads, normalized against the zero core shift model, no significant changes in runout was calculated in this simplified model. The plot also shows that it is more critical to control inboard runout, since outboard runout actually shows less thermally induced displacement in the z direction than a perfect model.

The second analysis varies core shift from -1.5 mm to 1.5 mm, while holding thermal loading at a constant and uniform 150 °C across both braking surfaces. Normal core shift values in the brake disc model used generally have a maximum magnitude of 0.75 mm, so this analysis checks the effect of twice the accepted values of core shift [2]. The data displayed in Figure 12 is normalized against the data generated by a perfect rotor with zero core shift.

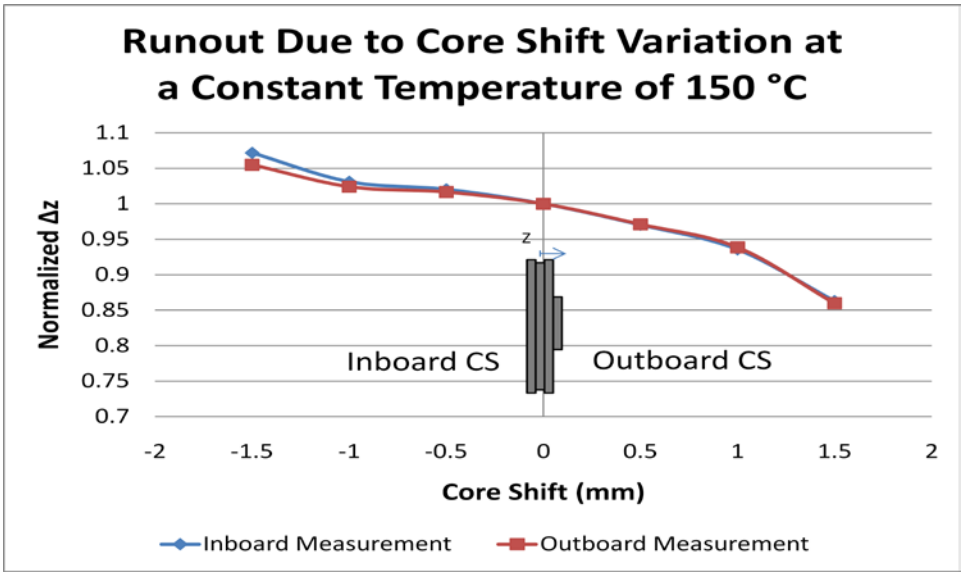

Figure 11: Effect on runout values due to varying core shift values at a constant thermal load, normalized against data from a 0 core shift model

An important result is that the variation of the displacement in the z direction is similar for both the inboard and outboard surfaces. This indicates that core shift in a perfect rotor with no surface inconsistencies does not generate additional DTV, when coupled with thermal loading. DTV from uneven

heating of the brake disc is a leading cause of hot judder [8]. The plot also shows that the manufacturing variation of core shift has a significant effect on runout, since increases in core shift correspond to a larger thermally induced runout. Once again, it can be seen that core shift towards the inboard surface of the rotor is more critical to reducing thermally induced geometric variation. However, this plot also shows that small increases in inboard core shift have less of an effect on runout than small increases in outboard core shift. Based on this study, it is important to reduce inboard core shift to reduce runout, but outboard core shift should also be avoided since it results in greater runout variation in large batches of discs.

Quantitatively, all thermal loading and core shift test models created for this analysis, with the exception of tests at a thermal load below 100 °C, showed a significant amount of runout. Most of these test scenarios showed a runout of 20 to 30 µm, which can lead to a high level of DTV through wear. A DTV of only 15 µm can be perceived as brake judder by an experienced driver [3]. Considering that a newly installed brake disc generally has runout on the order of 50 µm, an addition of half of this value due to core shift coupled with thermal effects is significant [4].

This study modeled a uniform thermal loading across both brake disc surfaces; whereas normal operating conditions coupled with pre-existing geometric variations of the brake surface usually cause localized hot spots or bands. Additionally, manufacturing processes seldom, if ever, create a uniform raising or lowering of the core, usually causing a tilting of the core within the mold instead.

3. ASSEMBLY RUNOUT

3.1 PROBLEM FORMULATION

3.1.1. Quantification of Assembly Runout

Brake disc runout has two sources, one of which is manufacturing deviations, such as core shift, and the other being assembly variations. There are many assembly parameter variations attributed to

causing runout, such as uneven lugnut torque and parallelism issues between the hub and rotor mounting faces. Additionally, caliper pressure and forces at the tire of the car can contribute to runout [7]. Parameter effects on runout investigated in this study are lugnut torque variation, indexing of the rotor, the tightening pattern and caliper pressure.

Runout can be measured using several different methods. In industry, runout is usually measured as a part of the imbalances in the rotor, rather than directly. The rotor is mounted horizontally and spun to detect imbalances, after which a balancing mark is machined into the disk to counteract any disproportion. Runout can be measured independently of other effects by mounting a dial caliper to the back surface of the rotor and documenting Δz, or peak-to-peak runout, during one full rotation. A more accurate measurement can be achieved by using a linear variable differential transformer (LVDT), or a non-contact distance probe, such as a capacitance or inductance probe. The common sensor used for rotor quasi-static rotor inspections is the LVDT [2].

3.1.2. Fundamental Questions

The experimental and FEM analyses of this study seek to answer several questions relating to runout causes:

- Which of the study parameters have an effect on assembly runout?
- How does an actual disc compare to a finite element model of a perfect disc in testing certain runout contributing assembly parameters?
- What type of experimental setup and procedure could be used in detecting assembly runout root causes?

3.1.3. Model Assumptions

Both the experimental and finite element analyses made assumptions in order to accomplish the task of assembly runout quantification. The results of assumptions made for the predictive experimental portion of this study are as follows:

- In comparison to normal operating conditions of a brake disc, a rotating speed of 60 rpm with no brake pressure applied and no tire mounted was taken to qualify as a static measurement of runout.
- Bearing stiffness was ignored, since it could not be controlled, and lumped with random error.

The results of assumptions made in creation of the finite element model include:

- An ideal disc with no runout or DTV present prior to pressure application was modeled.
- The bearing to rotor contact at the back of the hub was modeled by a zero translation boundary condition, although this may affect runout magnitude.
- In order to use the equation for calculation of bolt pressure on the face of the rotor, the following assumptions were made: standard threading with an average coefficient of friction due to average thread friction.

3.2 EXPERIMENTAL ANALYSES

3.2.1. Friction Experiment Setup

The dynamometer-type friction experiment used to run the static tests for the experimental analysis is built by the Acoustics and Dynamics Laboratory at the Ohio State University. It consists of a 5 HP Vector Drive electric motor with a 400 lb flywheel and a 32 in radius. Typical dynamometers used in industry couple the rotor through lugnuts instead of the shaft and have approximately 5 times more inertia [2]. Figure 13 shows the experimental setup on the dynamometer-type friction experiment.

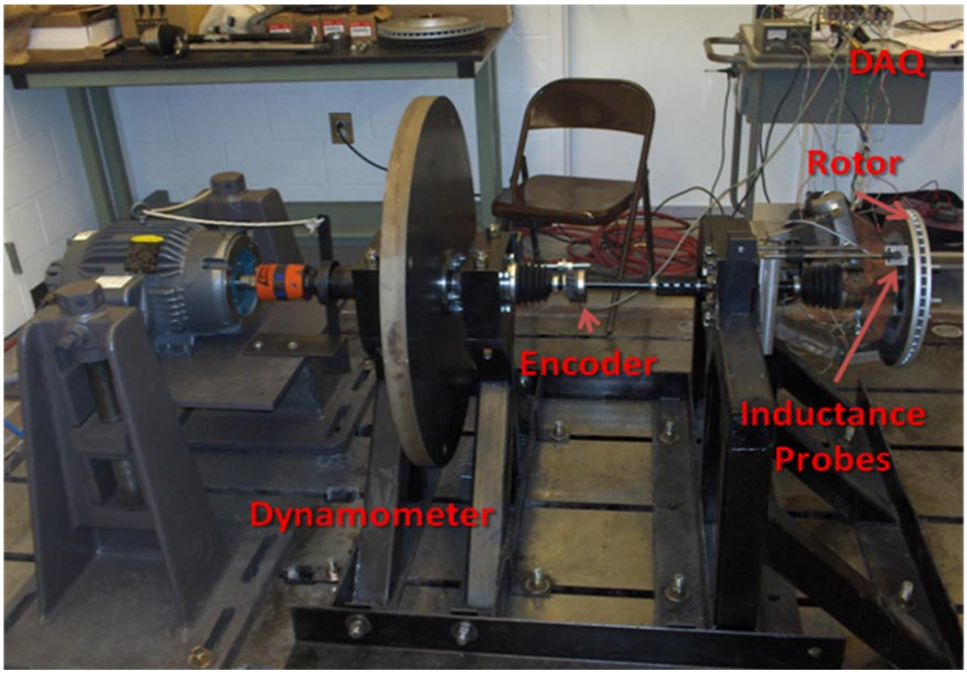

Figure 12: Picture showing dynamometer-type friction experiment setup

3.2.2. Measurement System

The measurement system used for experimental analysis consists of an encoder, two inductance probes and a pressure sensor for the calipers. A Model 25T Thru-Bore quadrature-type encoder with 2048 lines per revolution, manufactured by Encoder Products Company (EPC) is installed on the shaft between the flywheel and bearing. It uses a 5 V regulated Transistor-Transistor Logic (TTL) power supply. Two Omega LD701-1/2 inductance probes, with a regulated 24 V power supply are used to measure runout and the balancing mark, an indent on the outside edge of the rotor. The inductance probe setup is shown in Figure 14. They are mounted on the same radial line, with the runout probe at 1 in from the outer edge of the inboard braking surface.

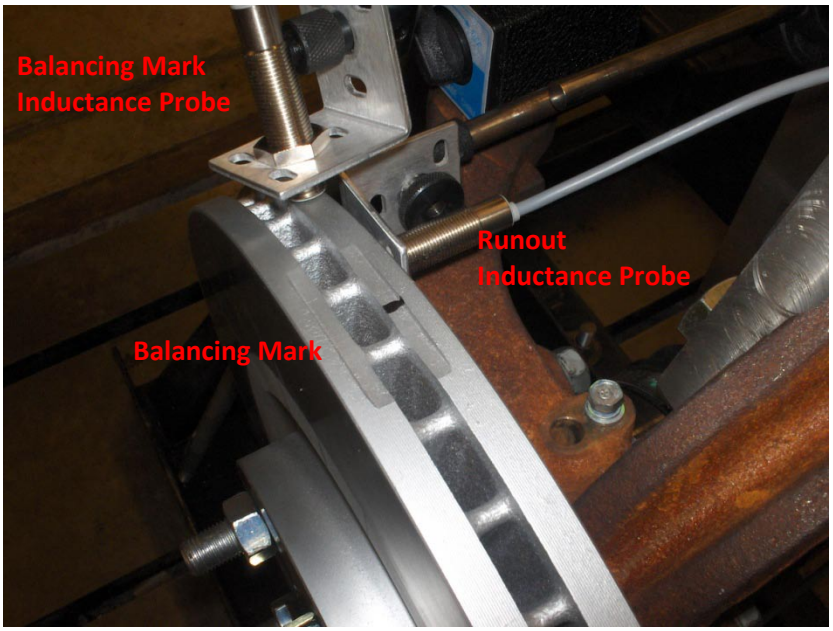

Figure 13: Inductance probe setup for experimental testing

They are designed to output a voltage when they are within a range of 2 to 5 millimeters of a surface made of mild steel but, since the rotor tested was made of gray cast iron, a calibration curve for the sensing distance was used. Section 3.4 on the inductance probes goes more in depth about this calculation. These probes have a repeatability of ±10 µm, which may have influenced data, since measurements are made on the order of micrometers.

A Honeywell Ratiometric pressure sensor is used with a 5V regulated power supply. It has a range of 0 to 1000 psi and incorporated in the hydraulic line between the caliper and master cylinder. The master cylinder is actuated by an external pneumatic cylinder controlled by a solenoid valve. The caliper and master cylinder setup can be seen in Figure 15.

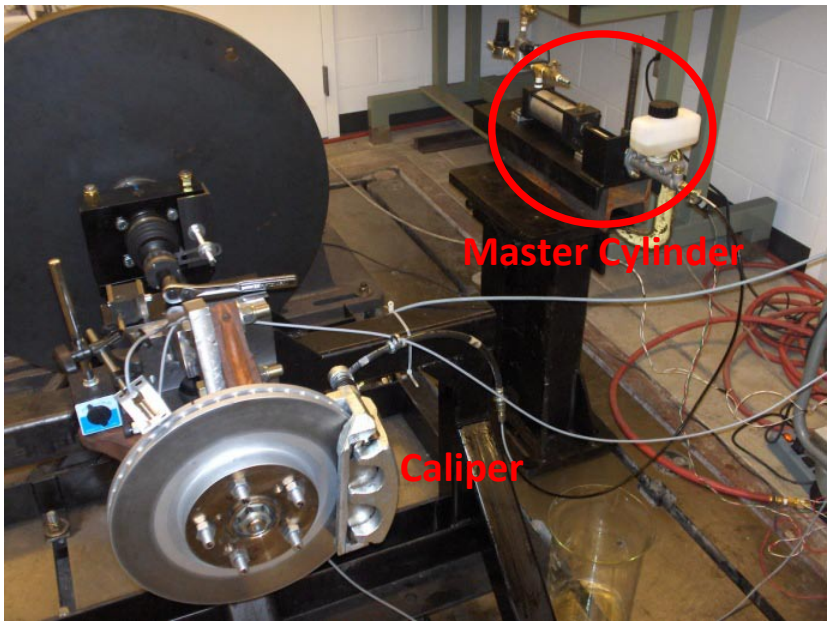

Figure 14: Picture showing setup of caliper and master cylinder

3.2.3. Data Acquisition System

The sensors used require an analog and a digital data acquisition system which are used with Labview as the input program. Both the inductance probes and pressure sensor use National Instruments (NI) 9239 analog input module in a CompactDAQ chassis. The encoder uses an NI 9411 digital input module, also in a CompactDAQ chassis.

The Labview front panel is shown in Figure 16. It has plots to monitor both the runout and balancing inductance probe output. It displays values of peak-to-peak run out in “MaxMin”, pressure in the caliper solenoid, runout read at the measurement position and current angle on the rotor from the encoder output. The “Avg” box shows the number of rotations counted after the program is started. The “Solenoid” switch puts pressure through the caliper to exert braking force on the disc. The “Record” switch is used to activate recording of data once the motor has reached steady state.

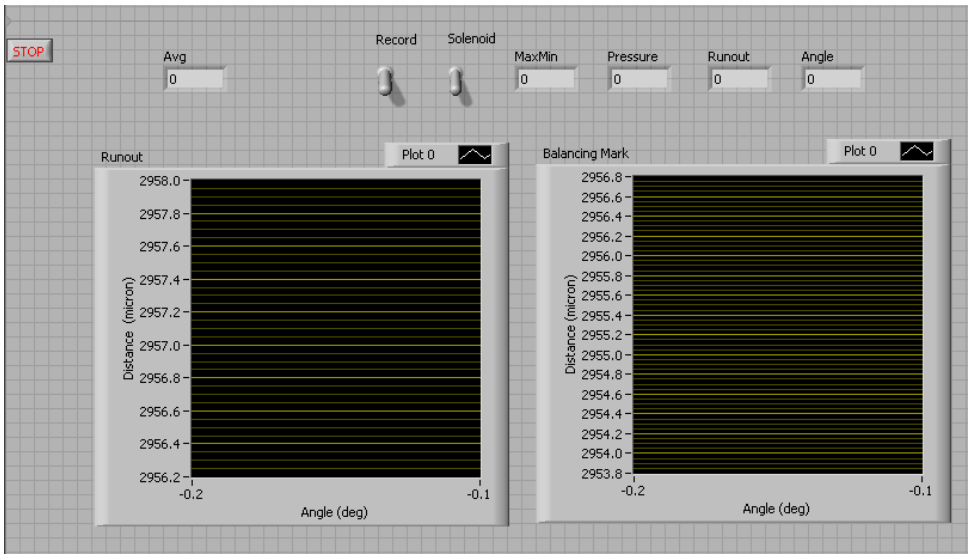

Figure 15: Labview front panel

The Labview block diagram can be seen in Figure 17. Data is taken from the encoder (digital signal) and inductance probes (analog signal) and written to a data file once the record switch has been flipped to the on position. The inductance probe data block actually holds all analog signals, including the pressure sensor signal. The runout, balancing mark and pressure sensor data are split out of this block. The runout signal is displayed, plotted against encoder angle in the front panel and used to calculate and display the total runout for the last rotation measured, or maximum to minimum runout. The balancing mark signal is plotted against encoder data and displayed in a front panel plot and the pressure signal is simply displayed. The solenoid switch is connected to a true/false block which will activate the caliper and exert pressure on the brake disc. The average counts the number of cycles of the program.

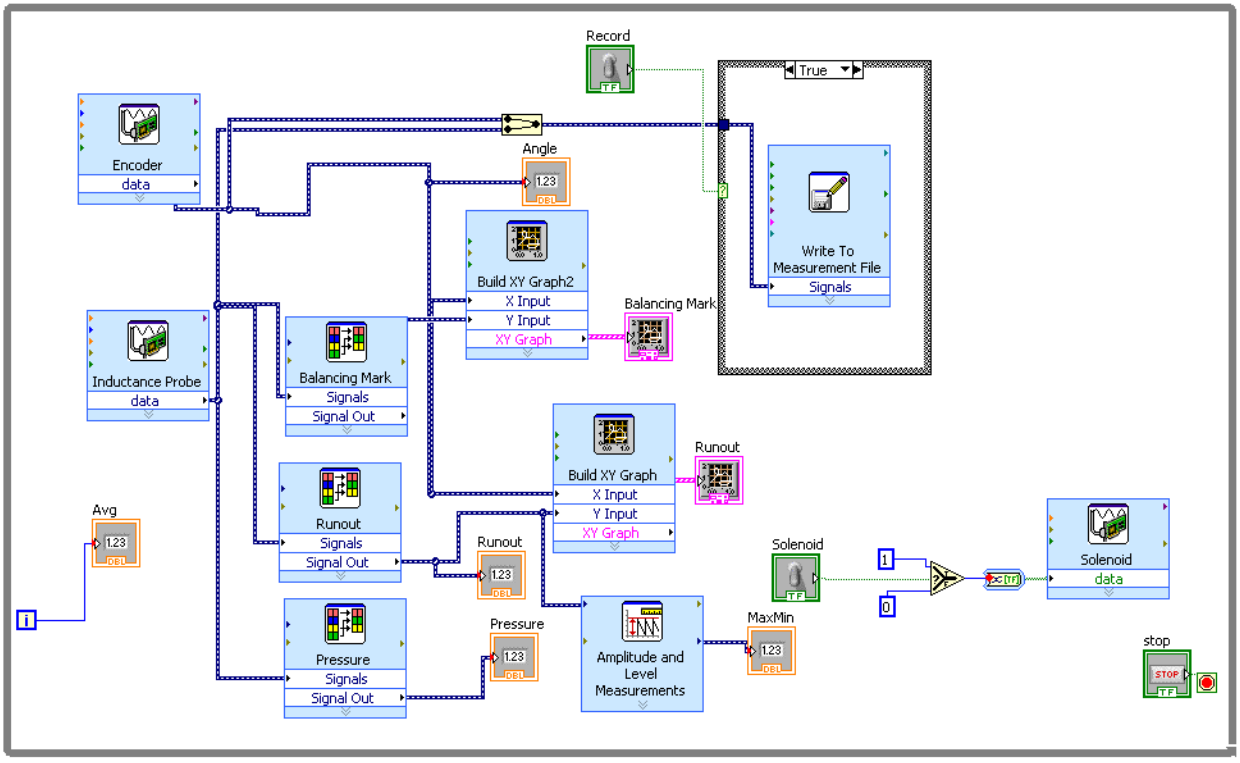

Figure 16: Labview block diagram

3.2.4. Induction Probes

Inductive probes are generally used as proximity sensors, rather than displacement sensors, but are ideal for the application of measuring runout in the brake disc rotor [13, 14]. They are compact, durable and inexpensive, have ideal sensing range for the application and good resolution. A non-contact displacement sensor is desired since an attempt with a dial caliper showed deviations in the measurement due to friction effects between the sensor and braking surface. Since a new brake disc with no wear is used, an absolute maximum of 100 µm of runout were anticipated so a low range was desired. Capacitance sensors would have fulfilled the sensor specifications required but at a much higher cost than inductance probes.

The measuring mechanism inside an inductance probes is the sensing coil, driven by high frequency sinusoidal excitation [13]. When it is brought in close proximity of a conductive material the magnetic field near the sensor is changed, leading to a change in the oscillation of the coil [13, 14].

Resolution of the coil is also changed when it is brought close to a metallic target. A demodulator compares the resolution of the sensing coil to a reference coil, creating the output voltage that is translated into a distance measurement using the calibration curve [13, 14].

The inductance probes used for the experimental analysis are designed for use with mild steel targets, so a calibration curve had to be obtained in order to use them for gray cast iron. While the data sheet lists an output voltage of 1 to 9 V, a test done by placing the sensor directly against the rotor and then out of range of any metallic target shows that the actual output ranges from 0.05 V to 9.85 V. A series of plastic shims were placed between the probe and the rotor to create the most accurate calibration curve. The resulting linear calibration curve is shown in equation 3,

$$y(micron) = 62.759x(V) + 873.38 \quad (3)$$

where is *x(V)* is the sensor output in volts and *y(micron)* is the sensor output in terms of microns of displacement.

3.2.5. Experimental Analysis of Parameters Contributing to Runout

A static predictive experimental analysis has been completed, varying three different parameters hypothesized to contribute to brake-disc runout. Data was taken in a total of twenty-eight experimental tests, with the first sixteen used for statistical analysis and the remaining eleven used primarily for verification and correlation to the FEM. Three parameters are varied, each at two discrete levels, leading to a total of eight setups to run each combination of parameters.

The three parameters varied are bolt tightening torque, bolt tightening pattern and indexing of the rotor relative to the hub. Tightening torque, as suggested by Original Equipment Manufacturer (OEM) specifications, is varied between 86 ft-lb and 101 ft-lb, the minimum and maximum accepted torques for assembly of the brake disc experimentally tested. The two tightening patterns tested are a clockwise pattern, characterized as tightening bolts sequentially around the circle, and a crossed

pattern, defined by tightening bolts opposite each other until all have been tightened. Figure 18 illustrates the order of tightening for each of the tested tightening patterns.

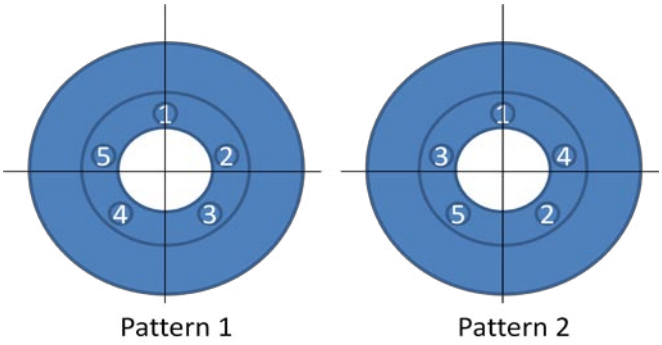

Figure 17: Bolt tightening patterns to be varied as a key parameter for the experimental analysis (numbers corresponding to order in which bolts are tightened)

Since the rotor has five bolts, indexing of the rotor is accomplished by rotating the brake disc 72°, or the holes clockwise to the next available bolt. Figure 19 shows a diagram of the indexing of the rotor.

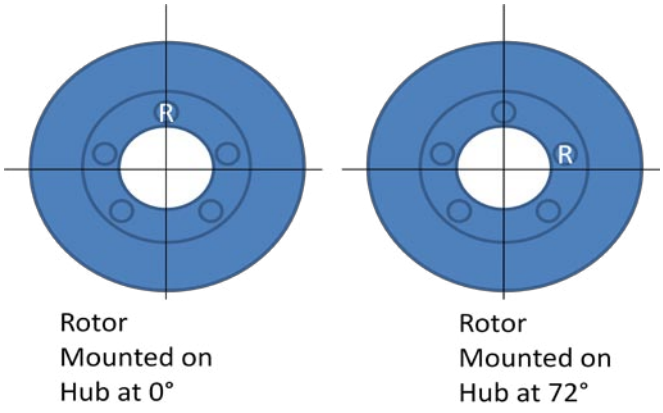

Figure 18: Indexing of the rotor to be varied as a parameter for experimental analysis, where R is the reference for rotor orientation

The test runs were completed in three different sessions, with those subsequent to the first seventeen completed after an initial analysis had been completed and more targeted scenarios could be tested. Initially an appropriate test setup had to be identified, so on the first day two different setups were attempted with the second being the one chosen. The first three experimental tests were completed on the first day, with the remaining thirteen used for statistical analysis and an experiment using caliper pressure completed on the second day. An initial data analysis was then completed and

further testing was scheduled approximately two weeks after the initial testing, with all remaining runs completed in a single day.

The experimental methodology was the same for each run, with the exception of the test with caliper pressure applied. The rotor was mounted on the hub, indexed at either 0° or 72° and the five lugnuts were tightened, using a torque wrench, to the correct torque and in the specified tightening pattern. After the rotor had been mounted according to experimental criteria to the bearing hub, the motor was turned on and allowed to reach steady state until the controller indicated its speed was 60 rpm ± 3 rpm. Data taking was activated in Labview, writing data from the encoder, pressure sensor and two inductance probes to a file. After approximately fifteen rotations of the rotor, data taking was stopped, before shutting the motor off. The seventeenth measurement, which incorporated caliper pressure, was run manually. The rotor was manually rotated 15°, as indicated by the encoder, and the runout displayed in the front panel of Labview was manually recorded. The caliper pressure was a constant 100 psi, applied opposite the inductance probe measuring runout.

Aside from the first sixteen measurements, the tests are designed iteratively, based on previous data. The first sixteen measurements are used for statistical analysis to determine which parameters have an effect on runout. They were randomly ordered to minimize bias error. The seventeenth measurement is used to check the effect of caliper pressure on assembly runout. After an initial analysis had been completed on these measurements, three test runs (18-20) were used to see if the experimental setup had changed before taking other measurement on the second test day.

Since the first 16 experiments all use constant loading, a correlation to the finite element model is beyond the scope of this project, so measurements 21 through 28 were devised for use in conjunction with the FEM. They are primary used to measure the effect of bolt tightening torque on runout values. Measurement 21 applies low torque to four lugnuts and high torque to the last lugnut, while measurement 22 applies high torque to two lugnuts and low toque to the rest. In measurement 23, the

torque on the lugnuts which had high torque in the previous run was increased by 20%. Measurements 23 through 28 are largely paired setups, where the rotor holes have the same tightening torque despite indexing of the rotor. For each of these pairs, the unequal tightening pattern rotates 72° clockwise with the rotor when it is indexed. Figure 20 illustrates how this applies to measurements 27 and 28, but measurements 23 through 26 are similar, whereby 25 and 26 repeat 23 and 24 in order to check repeatability of the experimental setup.

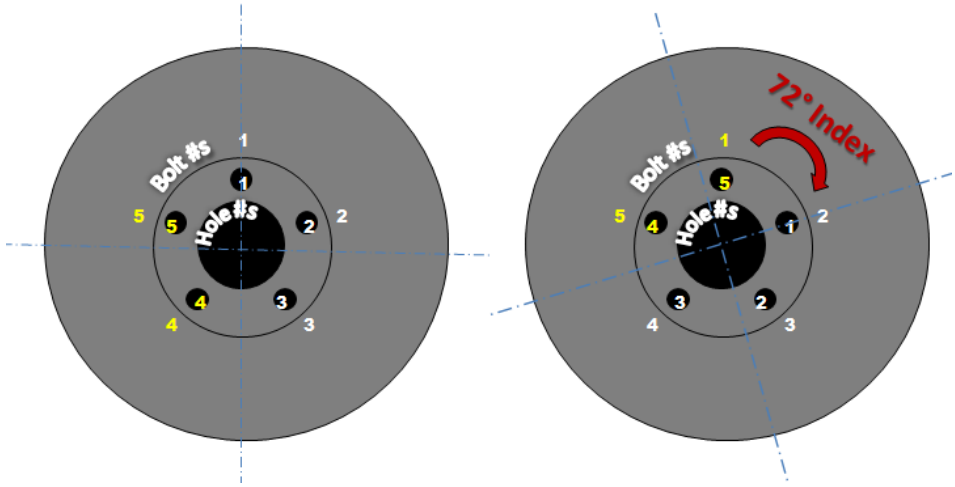

Figure 19: Diagram of runs 27 and 28 illustrating the bolt torque pattern, with yellow denoting removed lugnuts

These tests are completed in order to correlate to the finite element model. Table 2 shows a comprehensive listing of the experimental measurements completed in the analysis.

Table 2: Summary of measurements completed for the experimental analysis

Measurement	Parameters		
	Torque	**Tightening**	**Indexing**
First set of eight statistically analyzed runs			
1	Low	Clockwise	0°
2	Low	Crossed	72°
3	High	Clockwise	72°
4	Low	Clockwise	72°
5	High	Clockwise	0°
6	High	Crossed	0°
7	High	Crossed	72°
8	Low	Crossed	0°
Second set of eight statistically analyzed runs			
9	High	Clockwise	0°
10	High	Crossed	72°
11	High	Clockwise	72°
12	High	Crossed	0°
13	Low	Clockwise	0°
14	Low	Clockwise	72°
15	Low	Crossed	0°
16	Low	Crossed	72°
Caliper pressure of 100 psi at 15 degree intervals			
17	Low	Clockwise	0°
For comparison to statistically analyzed runs			
18	High	Clockwise	0°
19	*Low*	Crossed	0°
20	High	Clockwise	0°
Bolts 1-4 at low torque and 5 at high torque			
21	Low/High	Clockwise	0°
Bolts 1-3 at low torque and 4 & 5 at high torque			
22	Low/High	Clockwise	0°
Bolts 1-3 at low torque and 4 & 5 at 121.5 lb-ft			
23	Low/121.5	Clockwise	0°
Bolts 2-4 at low torque and 1 & 5 at 121.5 lb-ft			
24	Low/121.5	Clockwise	72°
Bolts 1-3 at low torque and 4 & 5 at 121.5 lb-ft			
25	Low/121.5	Clockwise	0°
Bolts 2-4 at low torque and 1 & 5 at 121.5 lb-ft			
26	Low/121.5	Clockwise	72°
Bolts 4 & 5 have nuts removed			
27	High	Clockwise	0°
Bolts 1 & 5 have nuts removed			
28	High	Clockwise	72°

3.3 COMPUTATIONAL ANALYSIS

3.3.1. Modeling Assembly Runout

Since Ansys has better meshing and contact control than SolidWorks Simulation, it was initially selected to do the FEM correlation but the version available was only capable of meshing 32,000 elements which was not adequate. The student version of SolidWorks Simulation can create a mesh of around 90,000 elements so it is used for this analysis instead. The finite element model is created in SolidWorks Simulation, using a model which John Drabison, a member of the Acoustics and Dynamics Laboratory, created by taking measurements of a rotor that had been halved for this purpose. The boundary conditions experienced on the dynamometer-type friction experiment are modeled by a fixed surface at the back of the hat and an elastic support with a stiffness of 2 E8 (N/m) at the inner radius of the hat. The load on the rotor due to lugnut torque is modeled as a pressure, calculated using equations 4 and 5 [10].

$$T = 0.2F_i d \qquad (4)$$

$$P = F_i / A_c \qquad (5)$$

In these equations T is the tightening torque, F_i is the force in the stud, d is the nominal diameter of the stud, or 14 mm, and A_c is the contact area between the nut and the rotor. The pressure corresponding to the low torque value of 117 Nm is approximately 377 MPa and the pressure for the high torque value of 137 Nm is 442 MPa. However, since the torque wrench has an error of ±25%, higher and lower torques are also analyzed using the FEM. The pressure calculation for all torques is shown in Table 3.

Table 3: Calculation of bolt pressure due to tightening torque

	Torque (Nm)	Fi (N)	P (MPa)
.+ 25%	146.25	52232.14	471.57
Low	**117.00**	**41785.71**	**377.26**
.- 25%	87.75	31339.29	282.94
.+ 25%	171.25	61160.71	552.18
High	**137.00**	**48928.57**	**441.75**
.- 25%	102.75	36696.43	331.31

Pressure Area (mm^2)	110.761
Pressure Area (m^2)	0.0001108

Figure 21 shows the meshed brake disc rotor with its boundary and loading conditions for a correlation to experiment 27 and 28. Similar boundary conditions are used for correlation to measurements 21 through 26, which have pressure across all five bolt holes.

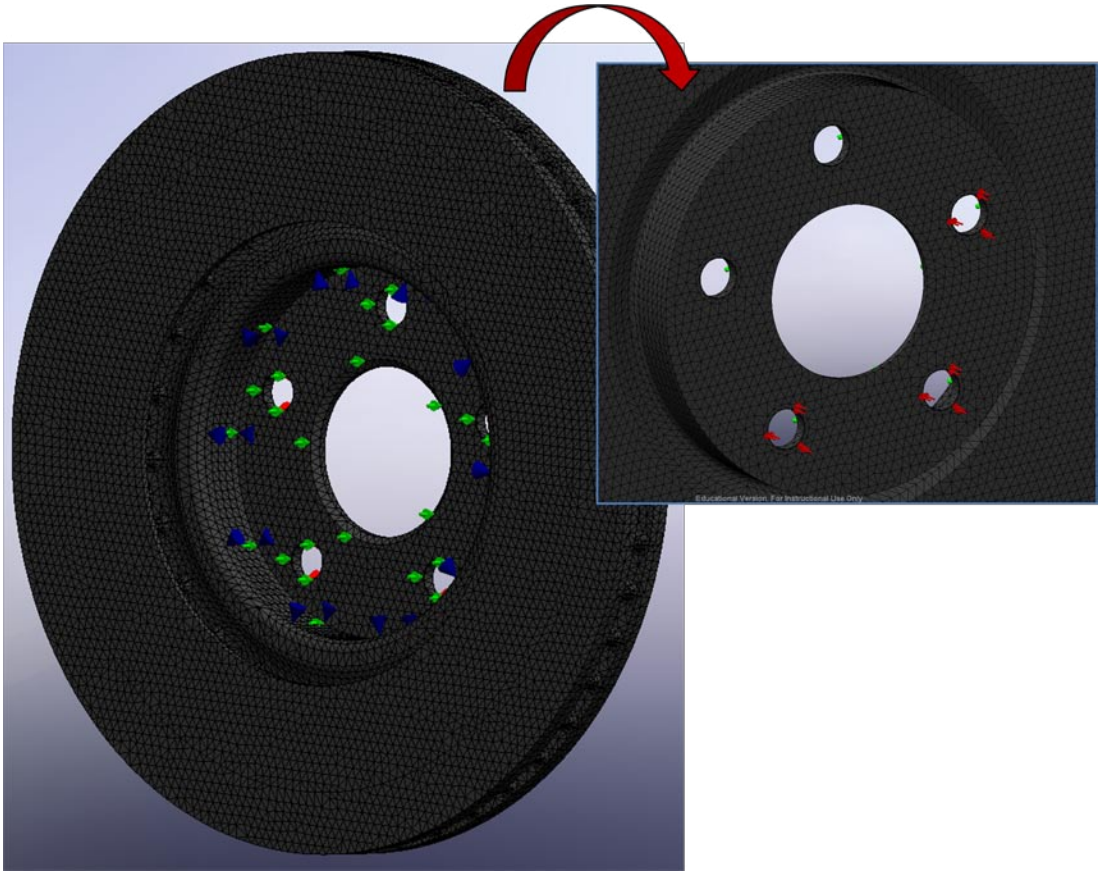

Figure 20: Brake disc rotor model showing the mesh as well as boundary and loading conditions

The caliper pressure model has the same boundary conditions at the hub, but with even pressure across the five holes and 100 psi pressure applied evenly across a caliper profile on both braking surfaces. The model can be seen in Figure 22.

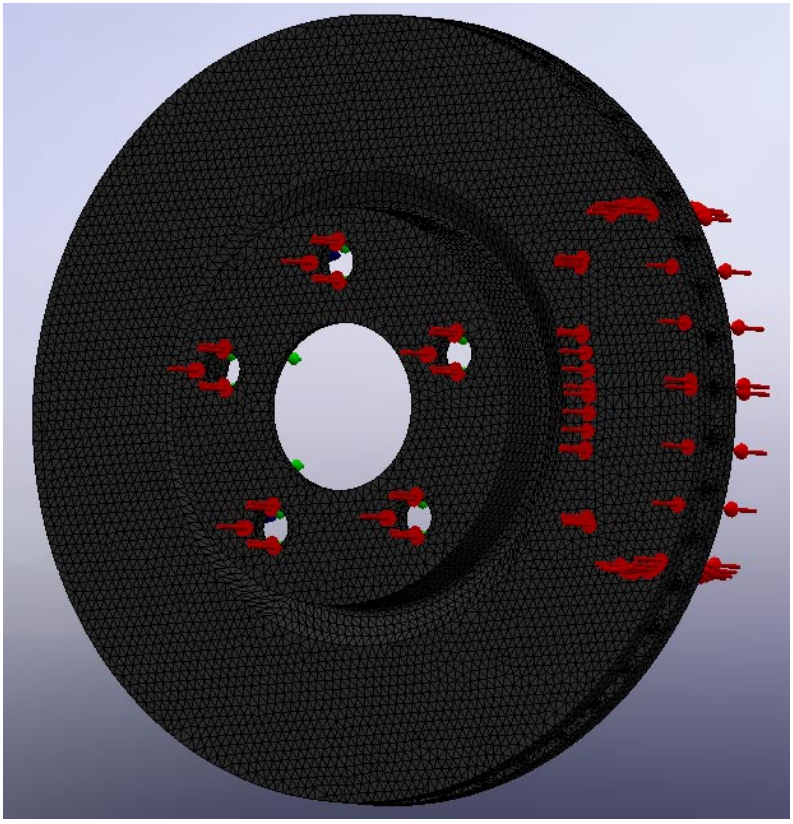

Figure 21: Meshed model showing FEM boundary conditions for correlation to the caliper pressure experiment (17)

In order to apply the pressures, the split lines feature with a projected curve is used. Although a mesh of 5 mm would have been adequate according to the convergence test, a mesh of 4 mm with 0.2 mm tolerance has been selected as it is the finest mesh possible without exceeding the element count available. Runout is measured at the inboard braking surface by using a probe along a circle concentric to the rotor edge and 1 in from the outer edge of the braking surface, since this models the placement of the runout measuring inductance probe most accurately.

3.3.2. Correlation between Experimental Results and Finite Element Predictions

Since the model is perfect with no manufacturing runout or DTV present, correlating the calculated results to symmetrically loaded measurements is outside the scope of this project as the test rotor has assembly runout. Therefore, of the three parameters experimentally tested, only torque level is analyzed by the FEM calculation. There is no reason to model indexing with a perfect rotor and symmetric boundary conditions, since it will have no effect on FEM runout. Tightening pattern could be modeled by creating small discrepancies between torque values on the modeled bolt holes, corresponding to the sequence in which they are tightened. However, this procedure would only yield useful results if the model had perfectly accurate boundary conditions. Therefore, the model is only used in correlation with measurements that have uneven bolt pressure, or experiments 21 through 28, and the measurement in which caliper pressure was applied to the rotor or experiment 17.

3.4 RESULTS AND DISCUSSION

3.4.1. Experimental Results

Normalized runout results for the first sixteen measurements, which are later statistically analyzed, can be seen in Figure 23. Values are normalized against the overall average. Since only two iterations of each combination of the three design parameters were measured, the population is too small to gage overall trends purely based on the averages plot of Figure 23. The statistical analysis is discussed in section 3.4.2 and shows more conclusive evidence of the effect of different parameters on runout.

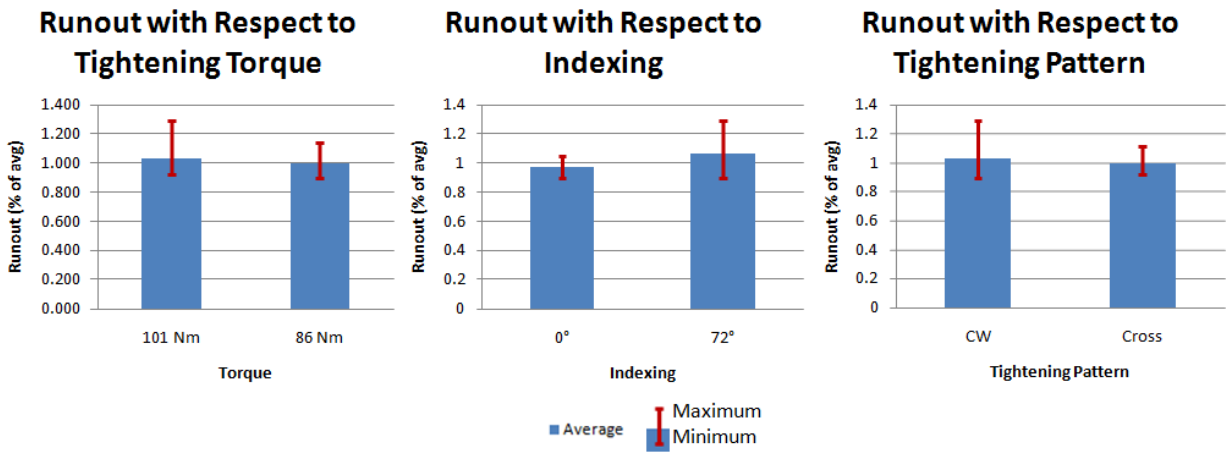

Figure 22: Average, maximum and minimum of each parameter normalized to the overall average runout measured

Although the brake disc was not mapped prior to experimental testing, the manufacturing runout sinusoidal profile is evident in runout plots. Figures 24 and 25 depict the manufacturing runout shape by showing representative plots at 0° and 72° indexing. A moving average trend line has been added to better show the general shape.

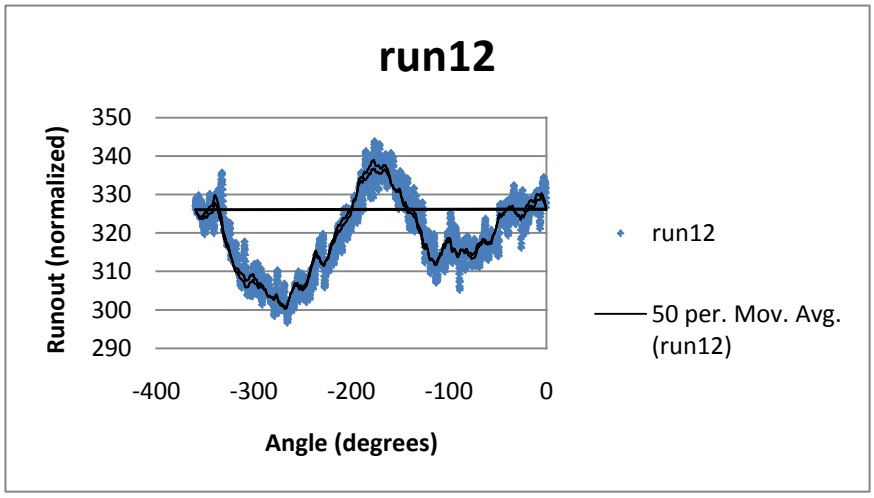

Figure 23: Representative plot of 0° indexed test runs with arbitrarily normalized runout

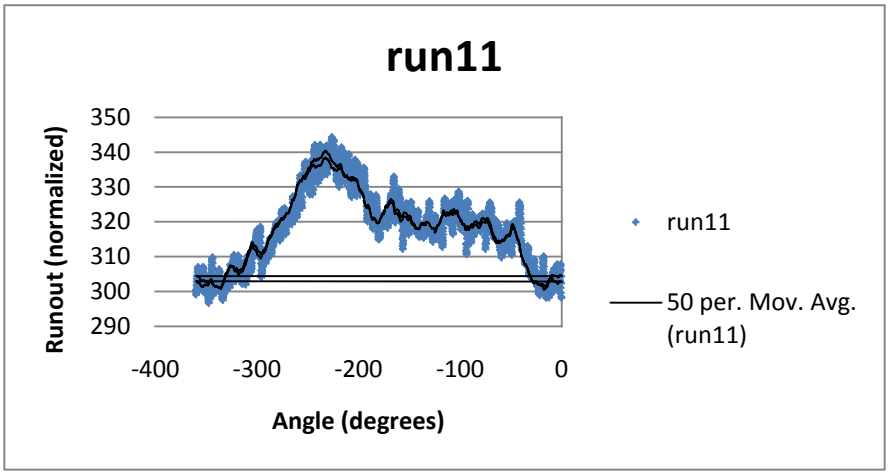

Figure 24: Representative plot of 72° indexed test runs with arbitrarily normalized runout

When the 0° indexed rotor runout plots are compared to 72° indexed plots, it is evident that indexing of the rotor has an effect on the runout profile. In Figure 26 it can be seen that removing the indexing from the measured data of run 11 shows that, although these two measurements had different assembly parameters, their shapes match up well.

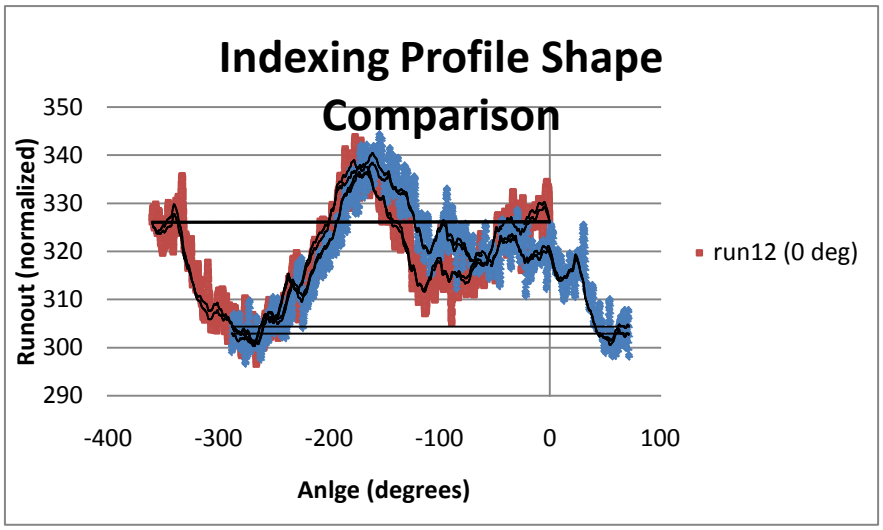

Figure 25: Runout profile comparison of 0 to 72 degree indexing with arbitrarily normalized runout

This curve shape is changed slightly by uneven bolt tightening, but retains a largely sinusoidal shape. This sinusoidal shape is typical of runout in new rotors, since it is usually caused by a runout angle that causes a tilting of the brake disc relative to the rotating plane [8].

Caliper pressure shows the same sinusoidal runout profile, since the test run checking the effect of caliper pressure was setup with a 0° index. Figure 27 shows the effect of adding caliper pressure to the experimental tests.

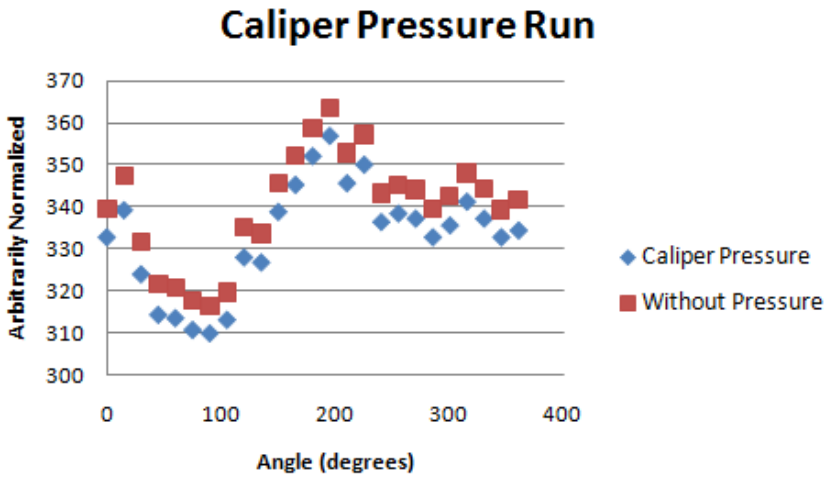

Figure 26: Test run 17 runout results with caliper pressure with arbitrarily normalized runout

The red points are measurements taken by the inductance probes directly before applying pressure, while the blue points are taken directly after applying 100 psi of braking pressure. Since the experimental setup shows variation, as indicated by later measurements, this was done to obtain a runout profile for direct comparison to the applied caliper pressure measurement. As the figure shows, caliper pressure causes a downward shift of the runout profile. This is due to the calipers pushing the opposite edge of the rotor (where runout was being measured) towards the inductance probe. A calculation of the peak-to-peak runout shows that caliper pressure caused a minimal decrease in runout of less than 1%. The magnitude of runout encountered during measurements is less than the average range for assembly runout on a new brake disc and the caliper test run is very close to the average. There is only a 3% difference between the caliper peak-to-peak runout and average runout, while isolated test runs have a difference up to 25%. In order to draw a more definite conclusion on the effect of caliper pressure as an assembly parameter additional test runs should be completed.

There are several sources of error in the experimental results, in addition to human and systematic error. Figure 28 shows the results of this error on measurements 23 through 26, which are two pairs of identical test runs, completed directly after one another.

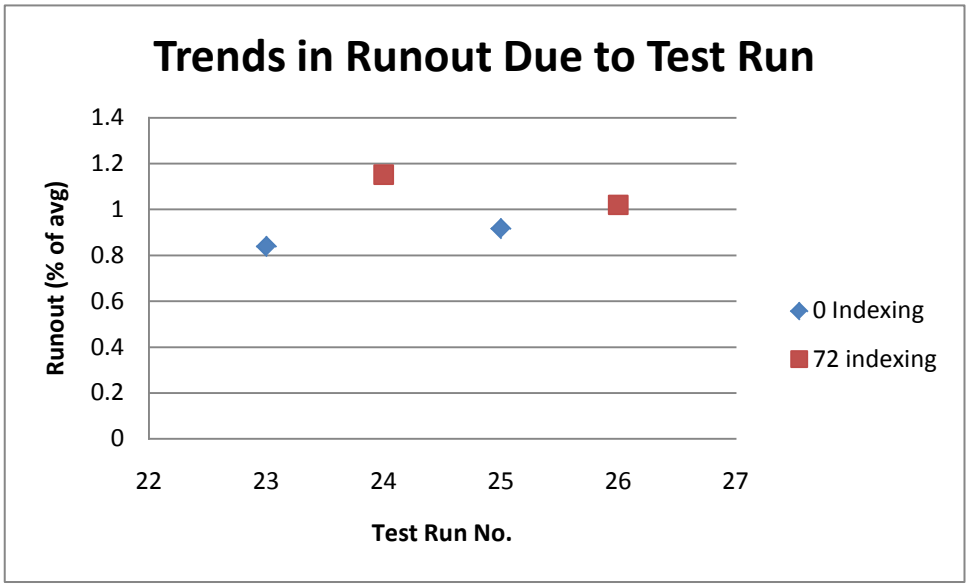

Figure 27: Repeated test runs, illustrating repeatability of the experimental setup

Since the rotor has to be removed in order to index it 72° between experiments, there are several possible sources of error that could contribute to this result. After the experimental measurements had been completed, it was discovered that the torque wrench has an accuracy of ±25% [15]. This range is only slightly better than error induced by hand tightening with a tool and there are many more accurate methods of measuring tightening torque, as can be seen in Table 4. The variation in torque is so great that it is designated as a random effect in the statistical analysis of experimental results.

Table 4: Error inherent in various torque measurment methods [15]

Accuracy	**Method of Measurement**
±35 %	By Feel
±25 %	Torque Wrench
±15 %	Turn of Nut
±10 %	Preload Indicating Washer
±1 %	Strain Gage
±15 % - ±8 %	Computer - Controlled Wrench
±3 % - ±5 %	Bolt Elongation
±1 %	Ultrasonic Sensing

The inductance probes may have also added to error of the experimental setup. The runout measurement location may not have been at the same radius for every measurement. Occasionally, during experimental setup the inductance probes were bumped and may have been repositioned slightly in the radial direction. In the second batch of test runs, a circle at 1 inch from the outer diameter of the rotor was drawn to ensure that the inductance probe was always placed correctly, but the first 16 tests were performed without this check tool. The probes themselves also have a repeatability of 0.01 mm, which is approximately 20% of the average runout measured.

3.4.2. Statistical Analysis of Measured Data

The effect of the variables of torque, index and tightening pattern on runout, spatial angle at minimum runout and spatial angle at maximum runout are analyzed using a mixed-factor three-way

ANOVA analysis using MINITAB software. A General Linear Model (GLM) has been fit to the runout amplitude (a), spatial angle at minimum runout (b), and spatial angle at maximum runout (c), and the resulting ANOVA tables are given below. Due to the large variation in torque control inherent to the torque wrench, this factor is defined as random and the index and pattern are defined as fixed factors [2]. According to the ANOVA on the runout amplitude, pattern is a statically significant factor (p-value < 0.05). According to the ANOVA on the spatial angle at minimum runout and maximum runout, index is a statistically significant factor (p-value < 0.05) [2]. The experiment was replicated for a better estimation of the random error in the model. For these experiments, the torque was run within the suggested OEM assembly specifications [2]. However, it is possible that with extreme cases of torque, the shape of the profile and associated runout will alter significantly, as seen in a later section comparing one such case with FEM results. The results of the ANOVA conducted can be seen in Table 5.

No post-hoc comparisons on levels are calculated due to the interaction with the random factor (torque) within the model [2]. However, the effect of indexing on shape of the profile is illustrated previously in Figure 24, by comparing two different traces.

Table 5: ANOVA tabular results; bold text shows p values showing relevant relationships

General Linear Model: Runout, Min Angle, Max Angle

Factor	Levels	Values
Torque random	2	86, 101
Index fixed	2	0, 72
Pattern fixed	2	10, 20

(a) Analysis of Variance for Runout, using Adjusted SS for Tests

Source	DF	Seq SS	Adj SS	Adj MS	F	P	
Torque	1	287.6	287.6	287.6	21.37	0.997	x
Index	1	66.1	66.1	66.1	0.17	0.754	
Pattern	**1**	**109.6**	**109.6**	**109.6**	**10441.01**	**0.006**	
Torque*Index	1	398.5	398.5	398.5	1.03	0.495	
Torque*Pattern	1	0	0	0	0	0.997	
Index*Pattern	1	24.4	24.4	24.4	0.06	0.843	
Torque*Index*Pattern	1	385	385	385	1.79	0.217	
Error	8	1718.3	1718.3	214.8			
Total	15	2989.5					

x Not an exact F-test.

S = 14.6556 R-Sq=42.52% R-Sq(adj) =0%

(b) Analysis of Variance for Min Angle, using Adjusted SS for Tests

Source	DF	Seq SS	Adj SS	Adj MS	F	P	
Torque	1	78	78	78	1.02	0.497	x
Index	**1**	**530119**	**530119**	**530119**	**6961.16**	**0.008**	
Pattern	1	2	2	2	2.41	0.364	
Torque*Index	1	76	76	76	82.05	0.07	
Torque*Pattern	1	1	1	1	1.02	0.497	
Index*Pattern	1	33	33	33	36.07	0.105	
Torque*Index*Pattern	1	1	1	1	0.02	0.881	
Error	8	311	311	39			
Total	15	530622					

x Not an exact F-test.

3.4.3. Finite Element Predictions

The finite element analyses completed shows a good preliminary correlation with experimental results. Since the modeled brake disc rotor has no manufacturing variation, all measured runout in the FEM is caused by assembly variations. Even loading is used in the convergence test for the model with the result that the 4 mm mesh used produces a runout of 0.0295 micrometers at the low torque value. Since the measurement system is not able to reliably measure such a small value it is not beneficial to compare FEM results to even loading experimental results.

The FEM calculations for experiments 21 though 28 show enough runout to be able to compare them to the experimental results. Table 6 shows the numerical runout results for these calculations, including additional models for runs 27 and 28, which calculate runout at torque values ±25% of the desired torque. This corresponds to the range that the torque wrench may have induced in the lugnuts.

Table 6: Runout percentage of the experimental average calculated by the computational FEM test runs 21 through 28 with torque wrench ranges for run 27 and 28

Test Run	Description	Runout (% of avg)
21	Bolts 1-4 at low torque and 5 at high torque	0.81
22	Bolts 1-3 at low torque and 4 & 5 at high torque	1.25
23/25	Bolts 1-3 at low torque and 4 & 5 at 121.5 lb-ft	3.09
24/26	Bolts 2-4 at low torque and 1 & 5 at 121.5 lb-ft	3.06
27 +25%	Run 27 with a 25% higher torque	11.15
27	Bolts 4 & 5 have nuts removed	8.92
27-25%	Run 27 with a 25% lower torque	6.69
28+25%	Run 28 with a 25% higher torque	11.20
28	Bolts 1 & 5 have nuts removed	8.96
28-25%	Run 28 with a 25% lower torque	6.72

The results show that the effect on runout of the torque wrench range is enough to affect the experimental results. Figure 29 graphically shows the effect on the full runout profile. The torque variation has a much larger effect on the peaks than the minimums since in these two tests there are only three lugnuts present. The minimum occurs at the part of the rotor where the bolts hold it most

securely to the bearing, modeled by a fixed surface at the back of the hat. Since it cannot move closer to the fixed surface without compressing, the majority of the runout occurs at the opposite edge, which is pushed away from the hub surface plane and measured as increases or decreases in runout due to torque.

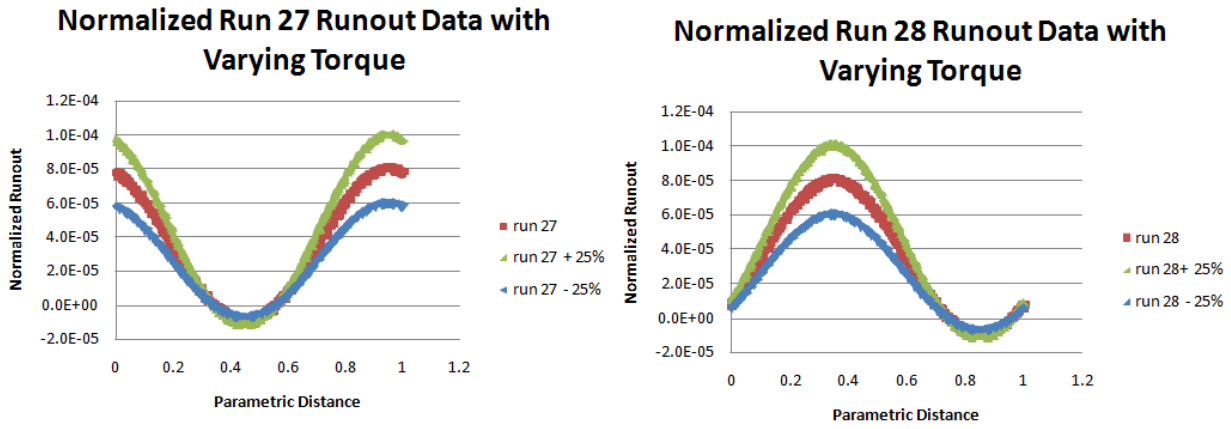

Figure 28: Effect of the torque wrench variations on runs 27 and 28

3.4.4. Prediction vs. Measurements

The sinusoidal runout profile found in measured results is also predicted by the FEM results of uneven loading of the bolt holes. The indexing has the same effect on FEM results as it does on experimental results, so that shifting one profile by 72° caused them to coincide, as can be seen in Figure 30.

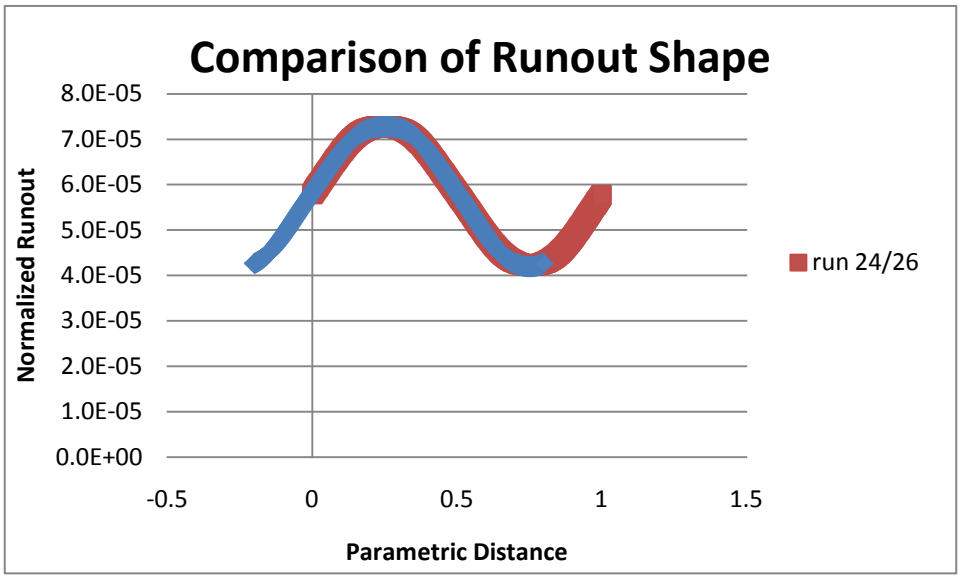

Figure 29: Comparison of FEM test runs to show that shifting profiles by 72° yielded similar results to those observed in experimental data

The profiles of the experimental results for the test runs with uneven bolt pressure have a different shape than other measurements. Since the FEM results show the increase in runout caused by uneven torque load on the rotor, subtracting this effect out of the experimental result should yield the shape of a representative measurement. However, finding the correct calibration factor and shifting the results to an appropriate angle is out of the scope of this project. Figures 31 and 32 show the measured representative and calculated FEM runout profiles, parallel to the experimental results for uneven torque loading for runs 23 through 28. Superpositioning a manufacturing runout profile with the FEM model, which shows pure assembly runout, should yield a plot similar the experimental results for uneven loading. In Figure 31 and 32, the manufacturing runout profile is substituted with a representative measurement since manufacturing runout was not measured prior to the experiment. The figures show how superposition of manufacturing and assembly runout could be achieved in future work to create a plot to compare to the measured results for uneven lugnut loading.

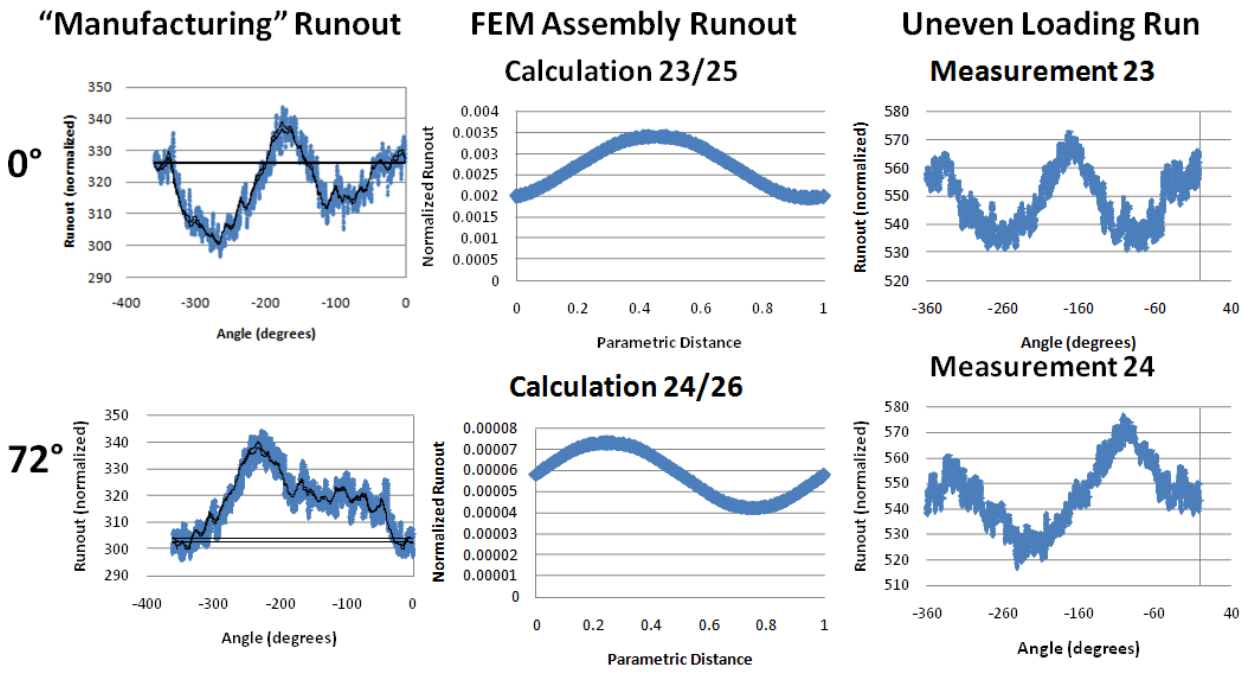

Figure 30: Correlation of FEM to experimental results, to be done in future work: the representative measurement represents the missing manufacturing runout profile, the FEM calculation is pure assembly runout and the measurement for uneven loading shows how a superposition of manufacturing and assembly runout would stack in runs 23 through 26

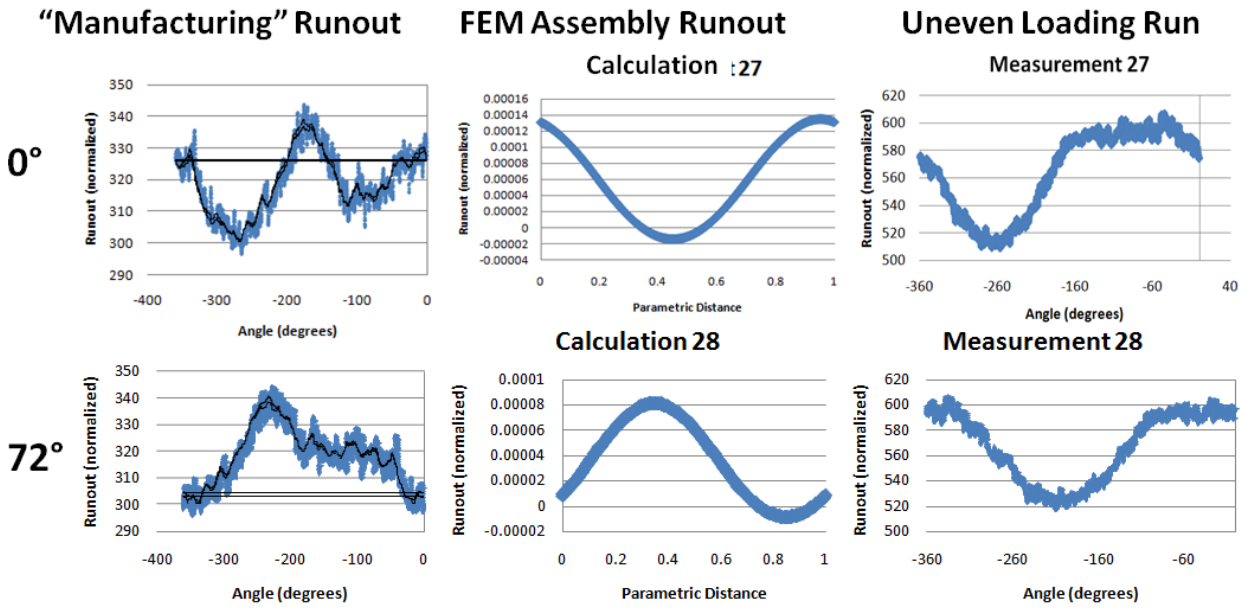

Figure 31: Correlation of FEM to experimental results, to be done in future work: the representative measurement represents the missing manufacturing runout profile, the FEM calculation is pure assembly runout and the measurement for uneven loading shows how a superposition of manufacturing and assembly runout would stack in runs 27 and 28

Only half of the measured runout profile for uneven loading appears to be affected at 0° indexing by the additional assembly runout caused by the uneven torque load. The same affect is observed in Figure 29, where changes in torque only affect the maximum half of the runout profile since the minimum half of the profile is the side that is attached firmly to the disc. At 72° indexing the profile is affected more drastically by the addition of uneven loading conditions. This is due to how the tightening load lined up with the manufacturing runout.

The other uneven loading experimental measurement which could be correlated to with the FEM was the caliper measurement. It is difficult to make a direct correlation to the experimental results with the FEM since the experimental results were measured differently than those obtained by the probe in the finite element model. In the experiment, the inductance probe measures the distance to the inboard brake surface at a static location relative to the disc and continues to take measurements at that location to get the entire radius of the disc. For uneven bolt loading, this measurement method is appropriate since the uneven load rotates with the disc. However, the effect of caliper pressure as an assembly parameter is not adequately measured by this approach since both the measurement device and caliper pressure are static relative to the disc. The probe in SolidWorks Simulation overcomes this problem by giving displacement of the entire radius at once, rather than a single location. However, the displacement directly at the caliper pressure profile is omitted in results. Figure 33 shows the C-shaped probe calculation radius and Figure 34 shows the resulting runout plot.

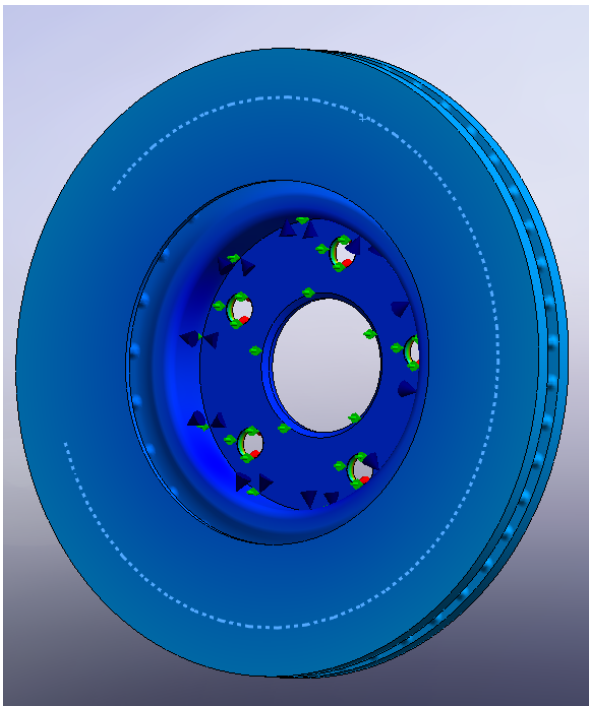

Figure 32: The dotted blue line shows the FEM runout probe calculation radius, with the location of the caliper pressure omitted

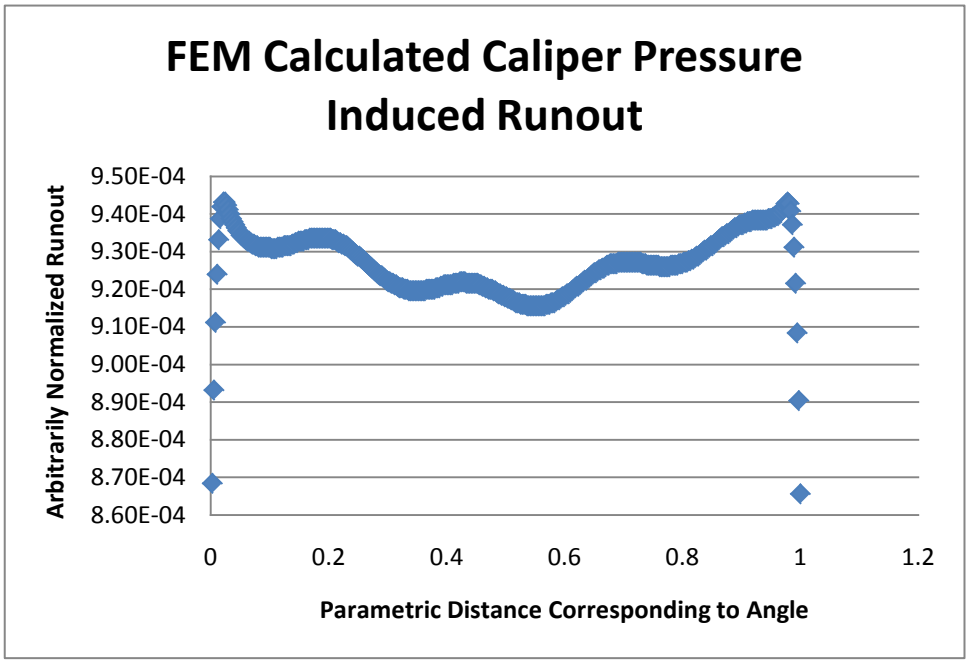

Figure 33: FEM-calculated runout profile on a brake disc model due to 100psi caliper pressure applied, the parametric distance corresponds to the angle of calculation with the drop off at either end showing where the caliper pressure was applied

Figure 34 shows the affect caliper pressure has on the entire runout of a perfect disc. The minimum runout occurs opposite the caliper pressure location, which could explain why the measured runout profile shifted down when caliper pressure was applied since the inductance probe was measuring near the minimum. Since the profile indicates an increase in runout near where the caliper pressure is placed, it appears that even an evenly applied caliper pressure causes a slight displacement away from the bearing at the pressure application point, due to rotor geometry. The FEM-calculated results cannot be directly correlated to the experimental results due to the measurement discrepancy. Comparing to a zero caliper pressure FEM model is also not appropriate since the even loading FEM shows minimal runout.

The boundary conditions in the finite element model will affect calculated runout magnitude. More realistic boundary conditions could yield different runout values since the contact pair between the bearing and rotor back surface may not be a 0 translation

4. CONCLUSION

4.1 SUMMARY

Parameters contributing to both manufacturing and assembly runout were investigated for their impact on overall runout. A basic finite element model was created to explore the significance of manufacturing variation in core shift, coupled with thermal effects. An experimental procedure for studying the effect of various assembly parameters on runout was established and used in correlation with finite element analysis.

Core shift, with friction heating, was found to have a significant effect on runout through various means. Core shift towards the inboard braking surface causes increased coning, a form of runout. The thermal load magnitude was shown to have little to no effect on runout magnitude, while increases in core shift caused a corresponding increase in runout. Interestingly, thermal effects, coupled with core

shift were found to have no effect on disc thickness variation in a perfect rotor without dynamic effects. Even at low temperatures the runout caused by core shift coupled with thermal effects was significant up to 50% of the accepted value for a newly installed rotor.

The experimental analysis identified parameters that have an effect on assembly runout. Indexing of the rotor relative to the hub was shown to be statistically significant to the location of the maximum and minimum runout measured and lugnut tightening pattern was found to be statistically significant to the peak-to-peak value of runout. The accuracy of the torque wrench prevented a definitive answer on the effect of tightening torque on runout. A comparison of the single caliper-pressure test to the rest of the data set leads to the assumption that caliper pressure does not induce a significant amount of runout. The typical sinusoidal runout profile was identified as the typical manufacturing runout profile. Superposition of a measured manufacturing runout with the FEM-calculated assembly runout may lead to better correlation to the experimental results of unbalanced torque pattern measurements.

An experimental procedure was designed and sources of error identified for future experimental work on brake disc runout.

4.2 RECOMMENDATIONS FOR FUTURE WORK

In this project, the experimental procedure was primarily used to identify assembly parameters that effect runout, but future work could be done measure these affects and identify additional parameters. Some adjustments should be made to the experimental setup in order to continue work. The torque wrench should be replaced with a more accurate tightening method, such as torque measured by a strain gage. It may also be beneficial to devise a more secure way of fastening inductance probes to minimize time between test runs to adjust slightly repositioned sensors, since they have such a small range. Additionally, if future experiments are to directly correlate experimental runout profile

results to each other fixed probes will be required to measure repeatable profiles. In the future, the rotor should be mapped for manufacturing runout prior to experimental test runs so that data can be better analyzed, experimental error can be identified and experiments can be designed based on current runs.

There are many additional tests which could be run with a modified experimental procedure. Addition of test iterations would allow for a more comprehensive analysis of runout values and distribution. It may also identify other factors to consider as runout affecting parameters. Inclusion of at least two separate levels of bearing stiffness to the experimental test runs would identify the importance of the bearings in assembly runout. The caliper test run should be repeated so that several iterations are available for analysis and at least two levels of pressure should be used. A separate measurement procedure along the radius of the disc would also yield more meaningful results. After runout effecting parameters have been identified, more in depth testing, with the addition of several levels, could lead to an understanding of trends in runout caused by each parameter.

The finite element analyses could be expanded and increased in complexity. First, more realistic boundary conditions must be used in order to get a better quantitative correlation. Although both the thermal and experimental FEM models used fixed surfaces, this is not realistic to actual operating conditions or dynamometer conditions. Substituting a boundary condition that includes the bearing stiffness would most likely result in more accurate results. The thermal loads in the core shift analysis should be changed to temperature gradients, taking into consideration vein cooling, center of friction gradient and caliper-position-induced gradient. A more accurate correlation to experimental results could be achieved by doing a superposition of measured manufacturing runout of a disc with FEM-calculated assembly runout to compare to experimental results of uneven loading tests.

An ultimate goal for future research projects might be to use experimental results to build a comprehensive finite element model that could represent a “real” disc with runout and DTV. It could incorporate static tests done in this project with thermal effects and actual operating conditions.

REFERENCES

[1] A. Leslie, “Mathematical Model of Brake Caliper to Determine Brake Torque Variation Associated with Disc Thickness Variation (DTV) Input”, SAE Paper No. 2004-01-2777, 2004.

[2] J. Dreyer, Conversations October 2009 to March 2010.

[3] H. Jacobsson, “Aspects of Disc Brake Judder”, IMechE Journal of Automobile Engineering, 217, 419-430, 2003.

[4] B. Breuer, and H. B. Karlheinz, editors, Brake Technology Handbook, First English Edition, Warrendale PA: SAE International, 2008.

[5] J. Kang, and S. Choi, “Brake Dynamometer Model Predicting Brake Torque Variation due to Disc Thickness Variation”, IMechE Journal of Automobile Engineering, 221, 49-55, 2007.

[6] H. Jacobsson, “Disc Brake Judder Considering Instantaneous Disc Thickness and Spatial Friction Variation”, IMechE Journal of Automobile Engineering, 325-342, 2003.

[7] K. Lee, and R. Dinwiddie, “Conditions of Frictional Contact in Disc Brakes and Their Effect on Brake Judder”, SAE Technical Paper Series, Warrendale PA: SAE International, 1998.

[8] T. Kao and J. Richmond, A. Douarre, “Brake Disc hot Spotting and Thermal Judder: An Experimental and Finite Element Study”, Inderscience Enterprises, Ltd., 2000.

[9] M. Groover, Fundamentals of Modern Manufacturing: Materials, Processes, and Systems, Third Edition, Danvers MA: John Wiley & Sons, Inc., 2007.

[10] R. Juvinall and K. Marshek, Fundamentals of Machine Component Design, New York: John Wiley & Sons, Inc., 2003.

[11] D. Bryant, and J. Fieldhouse, A. Crampton, C. Talbot, J. Layfield, “Thermal Brake Judder Investigations Using a High Speed Dynamometer”, SAE Technical Paper Series, Warrendale PA: SAE International, 2008.

[12] T. Valvano, and K. Lee, “An Analytical Method to Predict Thermal Distortion of a Brake Rotor”, SAE Technical Paper Series, Warrendale PA: SAE International, 2000.

[13] MicroStrain, Microminiature Sensors. “Non-Contact DVRT”. MicroStrain Inc: 2009. April 2009. <http://www.microstrain.com/ncdvrt.aspx>

[14] Fargo Controls Inc.. “Operating Principles for Inductive Proximity Sensors”. Fargo Controls Inc.: 1999-2009. April 2009. <http://www.fargocontrols.com/sensors/inductive_op.html>

[15] E. Obery and F. Jones, H. Horton, H. Ryffel, Machinery’s Handbook 26, New York: Industrial Press, 2000.